Published for SISSA by Springer

Received: October 14, 2022
Revised: December 8, 2022
Accepted: January 9, 2023
Published: January 26, 2023

JHEP01(2023)155

The sphaleron rate from 4D Euclidean lattices

Marc Barroso Mancha and Guy D. Moore

Institut für Kernphysik, Technische Universität Darmstadt, Schlossgartenstraße 2, D-64289 Darmstadt, Germany

E-mail: mbarroso@theorie.ikp.physik.tu-darmstadt.de, guy.moore@physik.tu-darmstadt.de

Abstract: We develop a new method to determine thermal activation rates, such as for bubble nucleation, topology change, etc., using 4-dimensional Euclidean methods. This allows nonperturbative study on the lattice. We then investigate the strong sphaleron rate in pure-glue QCD at temperatures between 1.3 T_c and 1000 T_c, making contact with previous results but extending them down close to the critical temperature. The extension to full QCD will be straightforward. Limitations of the proposal (the inability to compute a certain dynamical prefactor, puzzling large-volume behavior, and the inability to treat temperatures $T < 1.3\,T_c$) are also discussed.

Keywords: Lattice QCD, Finite Temperature or Finite Density, Non-Zero Temperature and Density, Quark-Gluon Plasma

ArXiv ePrint: 2210.05507

https://doi.org/10.1007/JHEP01(2023)155

Contents

JHEP01(2023)155

1 Introduction

Nonabelian gauge theories, including QCD and the $\mathrm{SU_w}(2)$ weak sector of the Standard Model, feature gauge groups which can have topologically nontrivial configurations in 4 spacetime dimensions [1–3]. Specifically, the spacetime integral of the contraction of the field strength tensor[1] $G_{\mu\nu}$ with the dual field strength tensor $\tilde{G}^{\mu\nu} \equiv \epsilon^{\mu\nu\alpha\beta} G_{\alpha\beta}/2$, satisfies:

$$q(x) \equiv \frac{\operatorname{Tr} G_{\mu\nu}\tilde{G}^{\mu\nu}}{16\pi^2}\,, \qquad Q_{\mathrm{I}} = \int \mathrm{d}^4x\; q(x) \;\in \mathbb{Z}\,. \tag{1.1}$$

[1]Our conventions are: we use natural units, $\hbar = 1$ and $c = 1$. The Euclidean metric is positive and the Minkowski metric is mostly-positive $g_{\mu\nu} = \mathrm{Diag}[-1, +1, +1, +1]$; the QCD/electroweak gauge fields are $G_\mu = G^a_\mu T^a$ and $W_\mu = W^a_\mu T^a$ with T^a the Hermitian fundamental representation Lie algebra generators, normalized to $\operatorname{Tr} T^a T^b = \frac{\delta_{ab}}{2}$; the fields take their geometrical normalization such that the gauge coupling does not appear in the covariant derivative $D_\mu = \partial_\mu - iG_\mu$ but as a denominator in the gauge action $\mathcal{L} = \ldots - \operatorname{Tr} G_{\mu\nu}G^{\mu\nu}/2g^2$.

That is, the integral of $q(x)$ the "topological charge density" always returns an integer, provided the integral is carried out over a compact domain without boundaries or with boundaries where the field strength goes to zero. (For the case of the $\mathrm{SU_w}(2)$ sector, replace $G_{\mu\nu} \to W_{\mu\nu}$.)

These topological structures are important because they lead to anomalies in axial quark number currents: according to the Adler-Bell-Jackiw anomaly [4, 5], each fundamental-representation fermionic species suffers a nonconservation of its axial charge in the amount

$$\partial_\mu J_5^\mu(x) = \ldots + 2q(x)\,, \qquad \Delta Q_5 = 2Q_\mathrm{I}\,. \tag{1.2}$$

Here J_5^μ is the Nöther current associated with axial quark number and Q_5 is the associated axial number. In the electroweak sector the effect is dramatic: because only left-handed species couple to $\mathrm{SU_w}(2)$, both baryon number and lepton number are violated, [3]: $\partial_\mu J_B^\mu = N_g \frac{\mathrm{Tr}\, W_{\mu\nu}\tilde{W}^{\mu\nu}}{16\pi^2}$ with $N_g = 3$ the number of generations. Topological transitions in real time can be stimulated if the fields can go over the so-called sphaleron barrier [6], and this process becomes efficient at high temperatures [7] and may explain the baryon number of the Universe (see for instance [8, 9] and references therein).

In Quantum Chromodynamics topological transitions in real time are also relevant for interesting high-temperature dynamics. They are responsible for the equilibration between right- and left-handed quark number in electroweak baryogenesis scenarios [10, 11]. In the context of relativistic heavy ion physics, noncentral collisions contain intense magnetic fields, which can combine with axial quark number imbalances to provide interesting new physics signals — the so-called chiral magnetic effect [12]. This proposal has inspired a great deal of work, including a deeper appreciation of the hydrodynamics of systems with axial quark number [13, 14].

Such chiral dynamics in QCD are very dependent on the decay rate of chiral imbalances. Close to equilibrium, a net axial charge abundance is described by a chemical potential for axial quark number μ_A; at leading order and in each quark species, the axial number density n_A is related to μ_A through [11]

$$n_A = \mu_A T^2\,. \tag{1.3}$$

The coefficient is determined by the quark number susceptibility, which is known [15] to be within 10% of the leading-order value already at $T = 2\,T_\mathrm{pc}$ with T_pc the pseudocritical temperature, $T_\mathrm{pc} \simeq 155\,\mathrm{MeV}$ [16, 17]. The axial chemical potential biases thermal transitions and thereby acts to create a net $G_{\mu\nu}\tilde{G}^{\mu\nu}$ value which drives down the axial number. The Minkowski time t_m derivative of n_A due to this thermal relaxation effect is:

$$\frac{\mathrm{d}n_A}{\mathrm{d}t_\mathrm{m}} = -\frac{\sum_f \mu_{A,f}}{T}\Gamma_{\mathrm{sphal},s} = -n_A\frac{n_f\Gamma_{\mathrm{sphal},s}}{T^3}\,, \tag{1.4}$$

where n_f is the number of light fermionic species and $\Gamma_{\mathrm{sphal},s}$, the so-called *strong sphaleron rate*, describes the equilibrium diffusion rate of topology due to random, real-time topological processes at temperature T:

$$\Gamma_{\mathrm{sphal},s} \equiv \frac{1}{Vt_\mathrm{max}}\left\langle\left(\int_0^{t_\mathrm{max}}\mathrm{d}t_\mathrm{m}\int_V \mathrm{d}^3x\, q(x,t_\mathrm{m})\right)^2\right\rangle = \int \mathrm{d}^4x\langle q(x)q(0)\rangle\,. \tag{1.5}$$

JHEP01(2023)155

That is, $\Gamma_{\mathrm{sphal},s}$ is the mean-squared topology per unit Minkowski 4-volume.[2] The definition is similar to the topological susceptibility χ_{top}, except that χ_{top} refers to correlators in Euclidean spacetime, while the time appearing in eq. (1.5) is real Minkowski time. As we will discuss below, these two rates have different physical interpretations and relevance and at high temperatures they strongly differ from each other.

In order to understand the dynamics of chiral imbalances, it is imperative to have at least a decent determination of the sphaleron rate $\Gamma_{\mathrm{sphal},s}$. If it is large, chiral imbalances relax quickly and are unlikely to lead to interesting dynamics. On the other hand, if it is small, it may be a good approximation to treat axial quark number as approximately conserved, at least for light species.

Unfortunately, the state of the art in determining $\Gamma_{\mathrm{sphal},s}$ is not very advanced. The equivalent $\mathrm{SU_w}(2)$ rate is relatively well understood. The relevant dynamics involves soft (wave number small compared to T) gauge fields which should behave like classical fields [18], though the relevant dynamics are subtle [19–21]. Building on early work by Ambjørn et al. [22], a fairly complete picture for the sphaleron rate in the $\mathrm{SU_w}(2)$ sector emerged by the end of the 1990s [21, 23–28]. This success is based on the fact that the $\mathrm{SU_w}(2)$ sector of the Standard Model has a rather small gauge coupling, $g^2N/4\pi \simeq 1/15$, which ensures that the relevant dynamics is quite infrared and the classical-field approximation is well under control. In comparison, even at electroweak temperatures $T \sim 1000\,T_{\mathrm{pc}}$, the strong coupling is of order $g^2N/4\pi \sim 0.3$, and the classical-field approximation is not very reliable. There are only two attempts to determine the strong sphaleron rate nonperturbatively using lattice techniques [29, 30], and the latter concludes that the results are no better than factor-of-2 estimates even at $T = 100\,\mathrm{GeV} \sim 700\,T_{\mathrm{pc}}$. The rate below this temperature is not even estimated.

We need a new approach to compute the strong sphaleron rate — one which does not rely on an approximation of QCD dynamics in terms of 3+1 dimensional classical fields. The approach must be nonperturbative, because the temperatures achieved in the early stages of heavy ion collisions are at most a few times higher than T_{pc}, where the theory is fully nonperturbative. Therefore the approach must involve our only rigorous tool for understanding QCD in this regime, which is 4-dimensional Euclidean lattice gauge theory.

One approach proposed recently [31, 32] is to measure $q(x)\,q(0)$ correlators as a function of Euclidean time and to attempt an analytic continuation to obtain the real-time spectral function, whose low-frequency limit determines $\Gamma_{\mathrm{sphal},s}$. This is an interesting approach, but it is very challenging, particularly because of our ignorance of the expected low-frequency behavior of the spectral function and the challenge in reconstructing nontrivial low-frequency structures in such analytical continuations.

We will provide a completely new approach for estimating $\Gamma_{\mathrm{sphal},s}$ from Euclidean lattice path-integral data. Our approach is based on the picture of thermal activation developed by Langer [33] and further developed by Affleck [34] and Linde [35, 36]. The next section (section 2) will review this picture. Thermal activation is controlled by Euclidean

[2] Some older sources define the sphaleron rate such that $dn_A/dt_{\mathrm{m}} = -\sum_{f,s}\mu_{A,fs}\Gamma/T$ where the sum also runs over spins s — that is, the sum is over all species which would be created by a sphaleron. This definition is half as large as the one we use, that is, $\Gamma = \Gamma_{\mathrm{sphal},s}/2$.

JHEP01(2023)155

configurations which are balanced at a saddlepoint between two (topological) minima, with a rate determined by the prevalence of saddlepoint configurations times the real-time rate that the fields move through such saddles. In subsection 2.2 we show that this rate is related to the size of fluctuations in the Euclidean direction, such that different Euclidean-time slices lie on different sides of the saddle. This is something which can be measured purely within Euclidean simulations. We formulate how to do this specifically for the QCD sphaleron rate (that is, SU(3) gauge theory with or without fermions) in section 3, and show how to really carry out such calculations in section 4.

With the method in hand, we make the usual checks for lattice spacing, lattice volume, and gradient-flow depth dependence, within pure-glue QCD (SU(3) Yang-Mills theory) in section 5. Having passed all tests, we explore what range of temperatures we can investigate in section 6, finding that the method breaks down below about $T = 1.3\,T_{\rm c}$. Our final results for temperatures above this threshold are presented in section 7, followed by a discussion and outlook.

2 Thermal activation: a review

The theory of thermal activation was pioneered by Langer [33] and put into field-theoretical language by Affleck [34] and by Linde [36]. The canonical example is the problem of bubble nucleation in a system with a stable and a metastable vacuum. At low or zero temperatures, this is controlled by a 4-dimensional bubble configuration, as argued by Coleman and Callan [37, 38]. At higher temperatures (roughly, when $1/T$ is of order or smaller than the diameter of the would-be 4D bubble), the relevant solution is instead a bubble which is constant in the (periodic, $\beta = 1/T$-extent, Euclidean) time direction and varies as a function of spatial radius. The field theoretical justification is worked out by Affleck [34] and by Linde [35, 36].

However, for our purposes this example is confusing and involves extraneous details. Instead, we will outline the key ideas, and motivate the approach we will take, with a much simpler toy example, proposed by Arnold and McLerran.

2.1 Simple example: pendulum under gravity

Consider a rigid pendulum in a gravitational potential. There is one degree of freedom φ, and the Lagrangian is

$$\mathcal{L}(\varphi, \dot{\varphi}) = \frac{m}{2}\dot{\varphi}^2 - V_0\,(1 - \cos\varphi)\ . \tag{2.1}$$

Arnold and McLerran used this problem to illustrate the difference between instantons and sphalerons and the physical role each plays [39], and we are guided by their considerations.

First, note that the energy spacing between the low-lying quantum excitations for this system is $\omega_0 = \sqrt{V_0/m}$, whereas the energy required to spin the pendulum over the top of its potential is $2V_0$. We will consider the case $2V_0 \gg \omega_0$ and will consider temperatures $T < \omega_0$, where the vacuum dominates, and $2V_0 \gg T \gg \omega_0$, where a range of thermal states participate but states with $E > 2V_0$ are still rare. To make the thermal ensemble make sense and the real-time behavior be more similar to a hot, chaotic system, we will couple φ

JHEP01(2023)155

to a thermal bath of oscillators. We assume that this bath causes a negligible modification of the above Lagrangian, but that it leads to noisy, dissipative real-time dynamics. We will not specify these couplings in detail, since this is only an illustrative example for us and not our main item of study.

Let us understand the distinction between instantons and sphalerons, and the role of each. First the instanton. The classical Lagrangian does not actually specify our problem completely, because the values $\varphi = 0$ and $\varphi = 2\pi$ (or any pair of values separated by 2π) are physically equivalent, and the wave function must be periodic up to a phase, $\Psi(\varphi+2\pi) = \Psi(\varphi)e^{i\theta}$. Here θ is a parameter, analogous to the Θ-parameter of QCD, which only plays a role in the quantum theory. Instantons are configurations which answer the question:

Instantons: how strongly does the free energy depend on θ?

We can address the θ-dependence of the free energy by considering its calculation with the Euclidean path integral. Naively we expect in the Euclidean path integral that φ is periodic, $\varphi(t=0) = \varphi(t=\beta)$, but in fact we only require periodicity modulo 2π. However, configurations with $\varphi(t=\beta) = \varphi(t=0) + 2\pi n$ should be weighted with a factor $e^{in\theta}$, such that the thermal partition function is:

$$Z(T) = \sum_{n\in\mathcal{Z}} e^{in\theta} \int_{-\pi}^{\pi} \mathrm{d}\varphi_0 \langle\varphi_0|e^{-\beta H}|\varphi_0 + 2\pi n\rangle = \sum_n e^{in\theta} Z_n(T)\,. \tag{2.2}$$

The φ_0 integral is a trace over all states, with the n-sum reflecting the fact that these states are 2π-periodic but allowing us to write a path integral in terms of states which do not have this periodicity. We name the configurations contributing to Z_n ($n \neq 0$) n-instantons.

At low temperature $Z(T) = e^{-\beta E_0}$ is dominated by the vacuum energy and the instantons determine how much the vacuum-energy depends on the boundary condition. For $\theta = 0$ all Z_n add and E_0 is minimized, as we expect for a periodic boundary, whereas for $\theta = \pi$ E_0 takes its maximal value because the vacuum wave function is forced to have a node at $\varphi = \pi$. At higher temperature the behavior is more complex. Even-parity (at $\varphi = 0$) states have the lowest energy for $\theta = 0$, but odd-parity states have the highest energy for $\theta = 0$ and the lowest energy for $\theta = \pi$. At temperatures well above $T = \omega_0$, the free energy is determined by a mixture of these states and the effects of θ tend to cancel out. In the Euclidean path integral, this happens because the characteristic t-width (Euclidean time width) over which φ varies in an instanton is $t \sim 1/\omega_0$. When $\beta\omega < 1$, the φ value must change very rapidly in order to complete an instanton, such that $S_{\text{inst}} \geq \int_0^\beta \mathrm{d}t\, m(\partial_t\varphi)^2/2 \geq 2\pi^2 mT$. The instanton action rises linearly at large T, rendering θ irrelevant. This point is illustrated in figure 1.

Now consider the same system, but distinguishing between $\varphi = 0$ and $\varphi = 2\pi$ as physically distinct configurations. In this case, we can consider a setup where the initial conditions are close to thermal, but with φ always close to the minimum at 0, and ask the completely different question:

Sphalerons: How fast does φ diffuse over the range of available $\varphi = 2\pi n$ minima over very long periods of Minkowski time?

JHEP01(2023)155

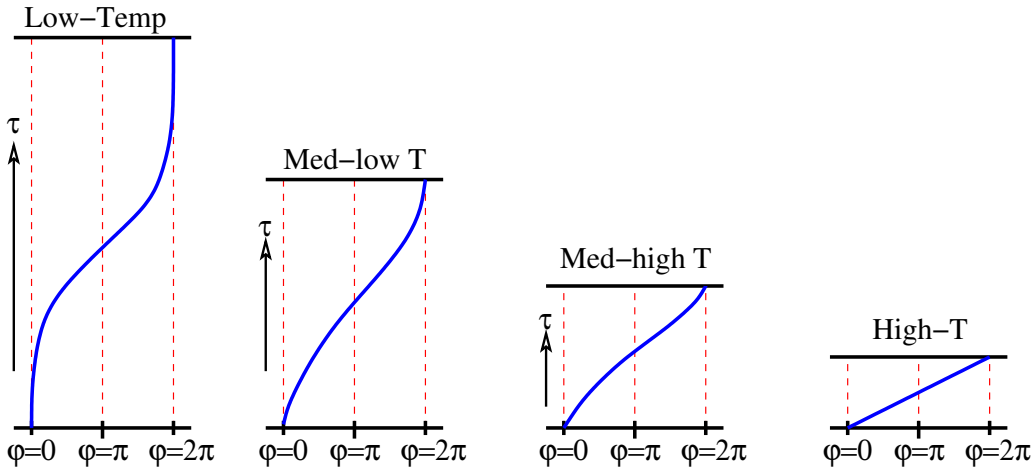

Figure 1. Instantons as a function of temperature. At low temperatures, φ transitions from 0 to 2π along a smooth characteristic curve. With increasing T, as the range of t-periodicity is narrowed, the instanton must "hurry" between $\varphi = 0$ and $\varphi = 2\pi$, increasing the associated action.

We can define this rigorously in terms of the long-time diffusion of φ's value, distinguishing between 2π-copies, as $\Gamma = \lim_{t_\mathrm{m}\to\infty} \frac{1}{(2\pi)^2 t_\mathrm{m}} \langle(\varphi(t_\mathrm{m}) - \varphi(0))^2\rangle$. This is controlled by transitions over $\varphi = \pi$ and its periodic copies because the potential has a maximum there and this represents the principal barrier to φ evolution.[3]

Intuitively, the sphaleron rate is the product of three factors (see figure 2):

1. How likely is φ to take a value near the top of the barrier? That is, what is $\mathrm{d}P(\varphi)/\mathrm{d}\varphi$ at $\varphi = \pi$, where $\mathrm{d}P(\varphi)/\mathrm{d}\varphi$ is the probability density to find φ in some narrow range about a specific value. In the toy model we expect $\mathrm{d}P/\mathrm{d}\varphi \sim \exp(-2V_0/T)$.

2. How fast does φ change values when it is at the top of the barrier? For our problem this is $\langle|\mathrm{d}\varphi/\mathrm{d}t_\mathrm{m}|\rangle$. Note that a rescaling of the variable φ changes both 1 and 2, but the change cancels such that the product of the two terms is rescaling invariant. In the toy model we expect $m\dot{\varphi}^2 \sim T$, so $\langle|\mathrm{d}\varphi/\mathrm{d}t_\mathrm{m}|\rangle \sim \sqrt{T/m}$.

3. How correlated are successive crossings of $\varphi = \pi$? This is a pure number, usually close to 1, which we will call $\mathbf{d}$.

The total transition rate is then

$$\Gamma = \left.\frac{\mathrm{d}P(\varphi)}{\mathrm{d}\varphi}\right|_{\varphi=\pi} \times \left\langle\left|\frac{\mathrm{d}\varphi}{\mathrm{d}t_\mathrm{m}}\right|\right\rangle \times \mathbf{d}\,. \tag{2.3}$$

[3]The definition of Γ described in footnote 2 is the rate of *forward* transitions, $\varphi < \pi$ transitioning to $\varphi > \pi$. The analogous rate is the relevant one for the bubble nucleation problem and is therefore the one considered by Affleck [34]. Again, the rate we consider is for transitions in both directions and is precisely twice as large. This factor emerges when computing $\langle|\mathrm{d}\varphi/\mathrm{d}t_\mathrm{m}|\rangle$, which is the mean rate of crossing in *either* direction. To compute the mean rate of forward crossings only, one should average this mean field velocity only over the forward-moving cases.

JHEP01(2023)155

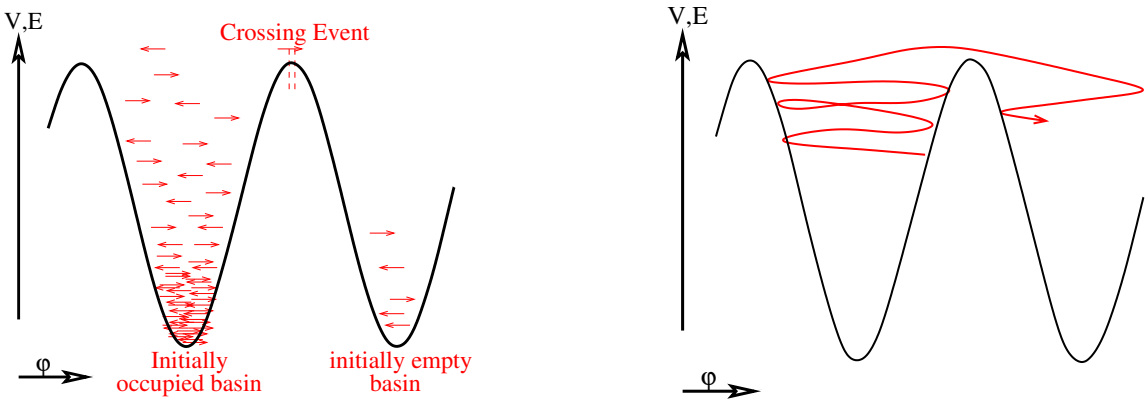

Figure 2. Cartoon of thermal activation in the pendulum toy model. Left: when one basin starts filled and one starts empty, the rate to move across is the flux across the top, which is the probability to be near the top times the rate of crossing. Right: for typical damping, an evolution bounces in one basin, gains enough energy to cross, and then bounces in the next basin.

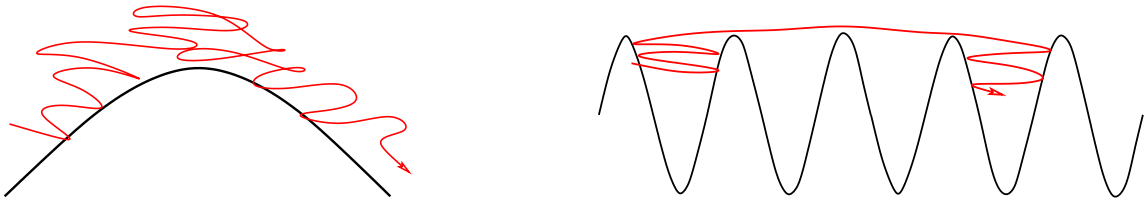

Figure 3. Cartoon illustrating the dynamical prefactor **d**. For extremely strong damping (left), the trajectory can cross the barrier several times in succession, leading to only one (or zero) true crossings. For underdamping (right), it can cross several barriers in succession.

The first two points are intuitively clear, but are explained in proper detail in the seminal paper of Affleck. The last point appears to have been first noticed by Arnold and McLerran [40], and is illustrated in figure 3. By very weak damping, the system can cross several barriers in succession. Crossings are positively correlated and the number of individual crossings underestimates the *square* of the change in $\varphi/2\pi$. In fact, in the absence of damping as considered by Arnold and McLerran [39], **d** is infinite and the mean-squared φ value rises quadratically, rather than linearly, with time. But for very strong overdamping, several crossings may occur in a single "macroscopic" crossing event — as appears to occur for the electroweak sphaleron rate [20, 21]. In this case, the true rate is smaller than the count of individual crossings. In a broad intermediate range of damping strengths, the $\dot{\varphi}$ direction does not change as it crosses the top of the barrier (say, the region where $V_{\rm max} - V < T$), but there is enough damping by the time it reaches the *next* barrier that it cannot cross. In this case we expect $\mathbf{d} \simeq 1$.

We should emphasize that the technique we develop here *cannot* determine **d**. Instead, we will concentrate on determining the product of the first two factors, and will assume that **d** is close to 1. This is a weakness of our approach, and it is not clear to us how it can be overcome.

JHEP01(2023)155

In a more general context, the exact location of and distance from the barrier may be harder to quantify. Therefore, a successful thermal activation calculation typically requires a few things:

1. Identify the "separatrix" which divides configurations into those closer to one minimum and those closer to another.
2. Identify some measure of distance φ from the separatrix.
3. Use a Euclidean path integral to find the probability to be within some narrow tolerance $|\varphi| < \Delta$ of the separatrix.
4. Determine the mean velocity of the φ variable when it is at or very near the separatrix.

We will show how to combine the last 3 steps into a single step, which does not require determining the value of φ.

2.2 Crossing speed and Euclidean fluctuations

How do we estimate $\langle|\mathrm{d}\varphi/\mathrm{d}t|\rangle$ (or its equivalent in more complex problems) using only Euclidean data? The answer lies in the size of the fluctuations in $\varphi(t)$ as a function of the Euclidean time t. The amplitude of these fluctuations is proportional to the rate at which φ changes in real time. After all, the real-time evolution can be determined by analytical continuation from the Euclidean-time dependence, as calculated in detail by Arnold and McLerran [39]. Consider again our toy example, with Lagrange function given in eq. (2.1). The Hamiltonian is

$$H = \frac{m}{2}\dot{\varphi}^2 + V_0(1 - \cos(\varphi)) \tag{2.4}$$

and classically, the thermal distribution of $\dot{\varphi}$ values is given by equipartition,

$$\begin{aligned} P(\dot{\varphi}) &\propto \exp\Big(-m\dot{\varphi}^2/2T\Big) \\ \left\langle\left|\frac{\mathrm{d}\varphi}{\mathrm{d}t_{\mathrm{m}}}\right|\right\rangle &= \frac{\int_0^\infty \mathrm{d}\dot{\varphi}\ \dot{\varphi} e^{-m\dot{\varphi}^2/2T}}{\int_0^\infty \mathrm{d}\dot{\varphi}\ e^{-m\dot{\varphi}^2/2T}} = \\ &= \sqrt{\frac{2T}{\pi m}}\,. \end{aligned} \tag{2.5}$$

For comparison, in Euclidean space, the dominant t-dependence in $\varphi(t)$ arises from fluctuations with Matsubara frequency $\omega = 2\pi T$:

$$\varphi(t) \simeq \varphi_0 + c\,\cos(2\pi t T) + s\,\sin(2\pi t T) \tag{2.6}$$

with φ_0 the average of $\varphi(t)$ over t values and c, s coefficients indicating two independent t-dependent fluctuations with this frequency. The action associated with these fluctuations is approximately

$$S(c,s) = \int_0^\beta \mathrm{d}t\ \frac{m}{2}(\partial_t\varphi)^2 = \int_0^\beta \mathrm{d}t\ 2\pi^2 m T^2\Big(c^2\cos^2(2\pi t T) + s^2\sin^2(2\pi t T)\Big) = \pi^2 m T(c^2+s^2)\,. \tag{2.7}$$

We can characterize φ's t dependence by looking at the RMS difference between $\varphi(t=\beta/2)$ and $\varphi(t=0)$, which equals $2c$:

$$\langle(\varphi(\beta/2)-\varphi(0))^2\rangle = \langle(2c)^2\rangle = \frac{\int_{-\infty}^{\infty} \mathrm{d}c (2c)^2 e^{-\pi^2 mTc^2}}{\int_{-\infty}^{\infty} \mathrm{d}c e^{-\pi^2 mTc^2}} = \frac{2}{\pi^2 mT} \;\Rightarrow\; \sqrt{\langle(2c)^2\rangle} = \sqrt{\frac{2}{\pi^2 mT}} \tag{2.8}$$

which is smaller than $\langle|\mathrm{d}\varphi/\mathrm{d}t_\mathrm{m}|\rangle$ by a factor of $1/T\sqrt{\pi}$. So the side-to-side fluctuations in φ are smaller than $|\mathrm{d}\varphi/\mathrm{d}t|$ by a factor of $1/T$, which one could guess on dimensional grounds, and an order-1 numerical factor.

Is this relation special? We claim it is quite general — the same Hamiltonian controls real-time evolution and Euclidean-time fluctuations, since the Hamiltonian H equals the Euclidean-time Lagrangian $\mathcal{L}_\mathrm{E}$.

To determine the numerical factor precisely, we have to decide precisely what question we want to ask about the Euclidean φ fluctuations. The point $\varphi=\pi$ separates values closer to the minimum at 0 and the values closer to the minimum at 2π, so we follow standard usage and call it a separatrix. In the following, it will be useful to ask how often $\varphi(t=0)$ and $\varphi(t=\beta/2)$ lie on opposite sides of this separatrix. In particular, we expect on the above reasoning that the first two terms in eq. (2.3) can be recast as:

$$\left.\frac{\mathrm{d}P(\varphi)}{\mathrm{d}\varphi}\right|_{\varphi=\pi} \times \left\langle\left|\frac{\mathrm{d}\varphi}{\mathrm{d}t_\mathrm{m}}\right|\right\rangle = \frac{\text{order-1 coeff}}{T} \times 2\,\mathrm{Prob}\Big(\varphi(t=0)<\pi<\varphi(t=\beta/2)\Big)\,. \tag{2.9}$$

Here $2\,\mathrm{Prob}(...)$ is the chance that φ is on opposite sides of π at the Euclidean times $t=0$ and $t=\beta/2$; the factor of 2 accounts for $\varphi(t=0)>\pi>\varphi(t=\beta/2)$.

To determine the order-1 coefficient, we must repeat the quick calculation of $(2c)_\mathrm{RMS}$ above with more care. We do so in appendix A, accounting for all Matsubara modes, finding that the real-time rate is $2T$ times the probability for $\varphi(t=0)$ and $\varphi(t=\beta/2)$ to be on opposite sides of the separatrix.[4] The appendix also shows how to include the effects of gradient flow, which we will need later.

The advantage of this formulation is that it is only necessary to determine which side of the "separatrix" $\varphi=\pi$ the field $\varphi(t)$ is on at the two (Euclidean) time values $t=0$ and $t=\beta/2$. When we try to apply these ideas to the sphaleron rate of QCD, we don't know how to measure the distance from the separatrix, but it is perfectly feasible to determine which side of the separatrix one is on.

One might worry that, in higher-dimensional problems like quantum field theory, the separatrix is generally a codimension-1 surface, rather than a single point. Does this approach still work? We argue that it does. At any point on the separatrix, one can find a local orthogonal direction and ask about motion, and fluctuations, in that direction.

[4] Here is a quick way to see why. Compare eq. (2.5) to eq. (2.8). The latter was computed with only the lowest Matsubara frequency, but all odd frequencies contribute, multiplying it by a factor of $\sqrt{\sum_{n=1,3,\ldots} n^{-2} = \pi^2/8}$. Also, eq. (2.8) is based on an RMS average, but we should compute the mean absolute value as used in eq. (2.5), which is smaller by $\sqrt{2/\pi}$ for Gaussian distributions. The two effects correct eq. (2.8) to $\sqrt{2/(\pi^2 mT)\times\pi^2/8\times 2/\pi} = (1/2)\sqrt{2/\pi mT}$ which must be multiplied by $2T$ to get eq. (2.5).

JHEP01(2023)155

At each such point, the speed a real-time configuration moves through the separatrix is determined by the same kinetic Hamiltonian as the Euclidean fluctuations orthogonal to the separatrix. Therefore, their relative amplitudes are proportional. The real-time Affleck-type calculation involves an integral over the separatrix surface of a local probability density times the local $\langle|\mathrm{d}\varphi/\mathrm{d}t|\rangle$, while our calculation involves the same surface average of $\langle\sqrt{\Delta c^2}\rangle$, which is proportional with fixed proportionality constant $1/2T$. Therefore, to the extent that configurations close to the separatrix really control the transition rate, the two calculations will be equivalent when the factor $1/2T$ is included.

3 Application to QCD

Let us see how to apply these ideas to the sphaleron rate in QCD. First, we will consider one more time an evaluation in the toy model:

3.1 Γ in the toy model

Before turning to QCD, suppose we were trying to determine Γ in the toy model, and we had a nonperturbative method for studying the finite-temperature Euclidean path integral. However, suppose we somehow could not access the exact value of φ, but only which side of π it lies on. We could perform our study as follows:

1. Generate a sample of typical Euclidean configurations:

2. For each, determine whether φ is on the opposite side of $\varphi = \pi$ at $t = 0$ as it is at $t = \beta/2$. This can be done by evolving $\varphi(t)$ under gradient-flow or relaxation dynamics and seeing whether it rolls down to $\varphi = 0$ or to $\varphi = 2\pi$, for instance.

3. Evaluate the sphaleron rate as $2T$ times the fraction of configurations which make such a transition.

To understand the approach, consider figure 4, which shows examples of how two configurations would be evaluated in this procedure.

The section from $t = 0$ to $t = \beta/2$ is cut from a simulation, and one "grafts" the gradient-flow path from the $t = 0$ configuration to the vacuum and from the $t = \beta/2$ configuration to the vacuum onto the two ends. The full configuration starts and ends at the zero-energy solution, $\varphi = 0$, *modulo* 2π. When the change is by $\pm 2\pi$, it is a sphaleron; otherwise it is not.

3.2 QCD: Chern-Simons number

Our approach in QCD will be the same: to look for configurations which cross a separatrix between $t = 0$ and $t = \beta/2$, and therefore settle into distinct vacua when acted on by gradient flow. There is no easily-measured value φ with a separatrix at $\varphi = \pi$ in QCD. However, we can use gradient flow and topology to define a separatrix and to give a measure which determines whether the $t = 0$ slice and the $t = \beta/2$ slice are on opposite sides.

JHEP01(2023)155

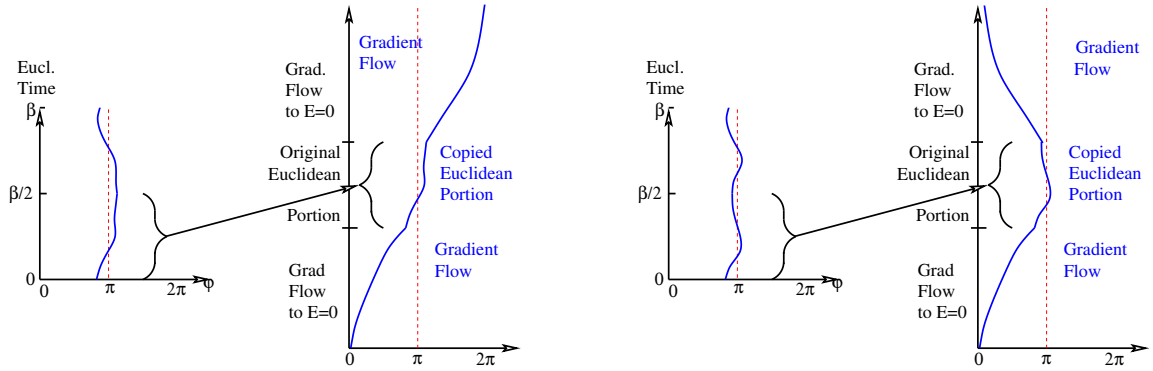

Figure 4. Cartoon of how two configurations would be evaluated using the gradient-flow approach described in the text. A segment of a Euclidean simulation, from $t = 0$ to $t = \beta/2$, is cut out of the simulation, and the starting/ending configurations are gradient-flowed to a zero-energy state. The whole path (zero-energy to $t = 0$ to $t = \beta/2$ to zero-energy) either has φ change by $\pm 2\pi$ (left) or by 0 (right); in the former case it counts as a sphaleron.

Let's start by defining gradient flow on a 3D configuration, in analogy to its usual 4D definition [41, 42]:

$$B_i(t, \vec{r}, \tau_{\rm F3} = 0) = G_i(t, \vec{r})\,, \qquad \frac{\partial}{\partial \tau_{\rm F3}} B_i(t, \vec{r}, \tau_{\rm F3}) = -\frac{\delta \int {\rm d}^3x\, {\rm Tr}\, G_{jk} G_{jk}[B]}{\delta B_i(\vec{r})}\,. \tag{3.1}$$

The fields $B_i(t, \vec{r}, \tau_{\rm F3})$, as a function of the 3D coordinate $\vec{r}$ and the 3D flow-time coordinate $\tau_{\rm F3}$, can be considered a 4D gauge-field configuration in the temporal gauge. One can then integrate the topological charge density over this 4D configuration:

$$Q(t) \equiv -\int_0^\infty {\rm d}\tau_{\rm F3} \int {\rm d}^3\vec{r}\; q(t, \tau_{\rm F3}, \vec{r})\,, \qquad q(t, \tau_{\rm F3}, \vec{r}) = \frac{\epsilon_{ijk}}{8\pi^2}\, {\rm Tr}\, G_{ij}\, \frac{\partial}{\partial \tau_{\rm F3}} B_k(t, \vec{r}, \tau_{\rm F})\,. \tag{3.2}$$

The result is equivalent to the definition of Chern-Simons number adopted in eq. (5) of ref. [43], which predates papers discussing 4D gradient flow [41, 42].

To understand $Q(t)$ better, consider an idealized 4D instanton solution centered at the origin, and consider a series of time slices through the instanton. For $t < 0$ slices, gradient flow will make the 3D gauge field roll down towards the vacuum described by the $t \to -\infty$ slice. This will yield $Q(t)$ values which change from 0 at very negative t towards $1/2$ for t close to zero. But on any $t > 0$ slice, the gauge field will gradient-flow down towards the vacuum described by the $t \to +\infty$ slice. Therefore, $Q(t)$ as defined above will have a sharp jump at $t = 0$ (the middle slice of the instanton), from a value around $+1/2$ to a value around $-1/2$. The slice where this jump occurs is our separatrix, and the property of the separatrix is that such a 3D slice, under gradient flow, moves to a saddlepoint between 3D vacua and sticks there.

Now return to the periodic (thermal) Euclidean path integral of time extent β. We want to know whether the $t = 0$ and $t = \beta/2$ slices are on opposite sides of this separatrix. We could evaluate $Q(t)$ as defined above at every time slice from $t = 0$ to $t = \beta/2$ and see if it makes a sharp jump. But this is inefficient. If we only want to know whether the $t = 0$

JHEP01(2023)155

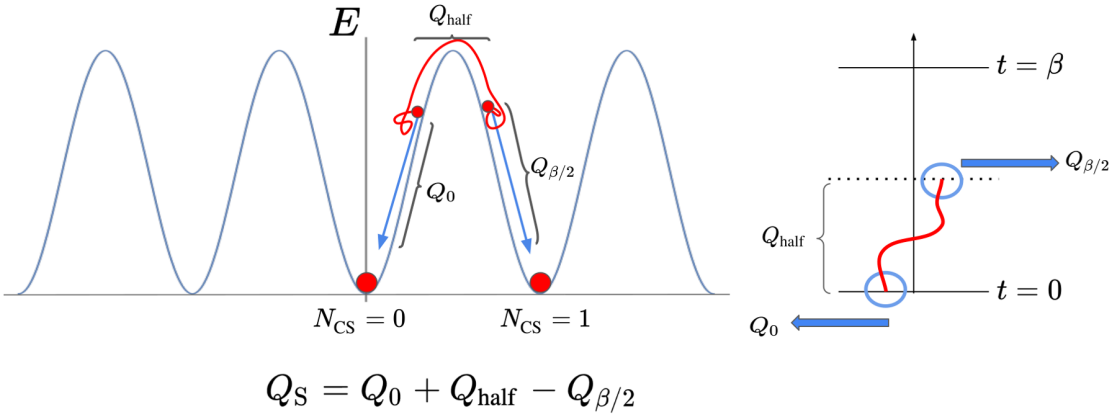

Figure 5. How we define and identify sphalerons in QCD. The topological density is integrated between $t = 0$ and $t = \beta/2$, and supplemented by its integration as these two boundaries are gradient-flowed to the vacuum. When the configuration crosses a separatrix, the result is ± 1.

and $t = \beta/2$ slices are on opposite sides, we can consider the following combination:

$$\begin{aligned} Q_{\text{S}} &= Q(t=0) + \left[\int_0^{\beta/2} \mathrm{d}t \int \mathrm{d}^3x\, q(x,t)\right] - Q(t=\beta/2) \\ &\equiv Q_0 + Q_{\text{half}} - Q_{\beta/2}\,. \end{aligned} \tag{3.3}$$

Here Q_{S} stands for the "sphaleron topology," not to be confused with $\int_0^\beta \mathrm{d}t \int \mathrm{d}^3x\, q(x,t) = Q_{\text{I}}$ the instanton topology of eq. (1.1). Q_{S} is "almost" the difference between $Q(t)$, defined above, at the two slices of interest. If we cross the separatrix, we expect Q_0 and $Q_{\beta/2}$ to be approximately $\pm 1/2$ and $\mp 1/2$ so the difference is ± 1. But by adding the q-integral over the intervening segment Q_{half}, we make the measurement actually topological. Namely, Q_{S} is the integral of $q(x,t)$ over a domain with no space boundaries (our box has periodic boundary conditions), which begins on a vacuum configuration at $t = 0, \tau_{\text{F3}} = \infty$ and ends on a vacuum configuration at $t = \beta/2, \tau_{\text{F3}} = \infty$, and has no field discontinuities in between. Therefore the integral of q, Q_{S}, is an integer. When this integer is nonzero, we define the configuration to be a sphaleron. This idea is illustrated in figure 5.

Lastly, note that the sphaleron rate is technically defined as the number of topology transitions per unit *time and volume*. Therefore, in defining the sphaleron rate, we must find the mean-squared value of Q_{S} from eq. (3.3), multiply by $2T$, and divide by the space volume which was studied — that is, $\langle Q_{\text{S}}^2 \rangle$ is expected to be extensive in the lattice volume, provided the lattice is large enough to see the large-volume behavior.

4 Lattice calculation of the sphaleron rate

As discussed in the last section, we will evaluate whether a given lattice gauge-field configuration is a sphaleron by evaluating Q_{S} defined in eq. (3.3), determining

$$\frac{\Gamma_{\text{Eucl}}}{T^3} = \frac{\langle Q_{\text{S}}^2 \rangle}{(N_s/N_t)^3}\,, \tag{4.1}$$

JHEP01(2023)155

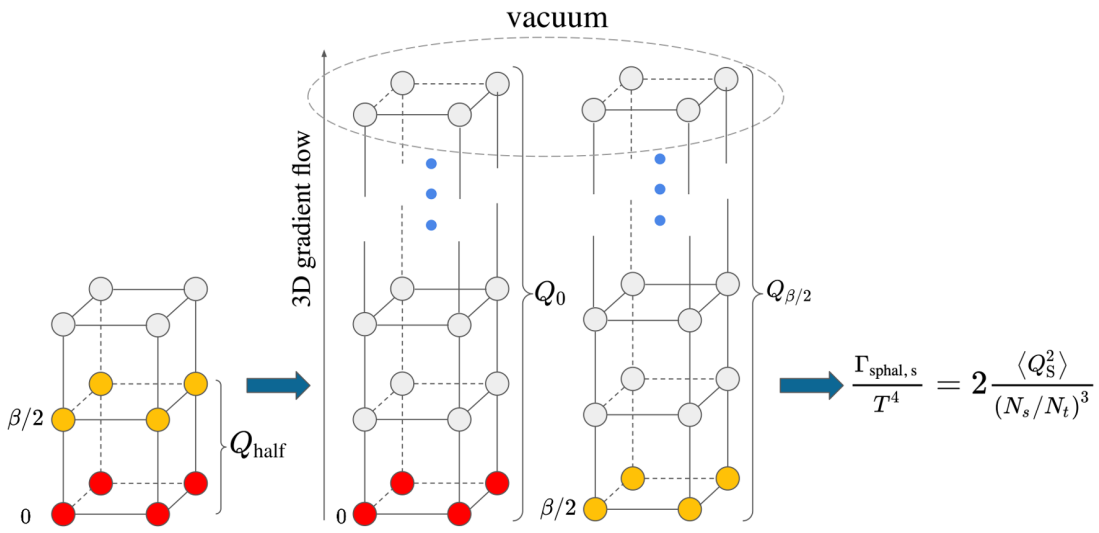

Figure 6. Sketch of the calculation performed on the lattice to determine the sphaleron rate. One dimension of the lattice is left not drawn for convenience.

with N_s and N_t the number of lattice points in the space and time directions respectively, and then rescaling by $2T$ to convert this into the real-time rate as described in the appendix, specifically eq. (A.15):

$$\Gamma_{\text{sphal},s} = 2T\Gamma_{\text{Eucl}} \,. \tag{4.2}$$

There is one additional complication which we must overcome to make the procedure work. Integrating $q(\vec{r}, t)$ on a lattice gauge configuration typically returns a highly noisy result, because the lattice definition of $q(\vec{r}, t)$ is contaminated with high-dimension operators which are not topological.[5] Therefore it is essential to apply some lattice gradient flow (Wilson flow [42]) on the 4D configuration before the evaluation. This 4D gradient flow also reduces the size of the fluctuations in the temporal direction which we discussed in subsection 2.2 and in appendix A. This will reduce how many configurations cross the separatrix and are counted as sphalerons. Appendix A.2 contains a calculation of the size of this effect, which we can use to correct for the effects of gradient flow.

Just to summarize the procedure, the steps that we need to take are the following:

1. Generate a valid lattice QCD configuration through a Hybrid Monte-Carlo algorithm.
2. Apply a certain amount τ_{F} of 4D gradient flow in order to reduce the UV noise.
3. Calculate the topology enclosed in half the lattice.
4. Extract the 3D slices at $t = 0$ and $t = \beta/2$, and compute $Q(0)$ and $Q(\beta/2)$ according to (3.2), using a 3D version of gradient flow all the way to the vacuum.
5. Calculate Q_{S} with these quantities, see eq. (3.3). Repeat for many configurations to extract $\langle Q_{\text{S}}^2 \rangle$.

The procedure for determining Q_S is illustrated in figure 6.

[5] We use the clover definition of $q(\vec{r}, t)$.

JHEP01(2023)155

		N_t					
		6	8	10	12	14	16
T/T_c	1.3	6.04979	6.23700	6.39495	6.53054	6.64889	6.75371
	2	6.33718	6.54976	6.72273	6.86803	6.99311	7.10283
	3	6.64031	6.86803	7.04966	7.20049	7.32939	7.44187
	4	6.86803	7.10283	7.28847	7.44187	7.57254	7.68632
	5	7.04966	7.28847	7.47640	7.63126	7.76294	7.87746
	7	7.32939	7.57254	7.76294	7.91939	8.05216	8.16748
	10	7.63126	7.87746	8.06960	8.22716	8.36070	8.47657
	20	8.22716	8.47657	8.67054	8.82926	8.96359	9.08003

Table 1. Value of the lattice coupling β_{latt} for different values of T/T_c (where T_c is the critical temperature of the pure-glue Yang-Mills theory, given by $T_c = 287.4(70)\,\text{MeV}$) and number of sites in the temporal direction N_t.

In this paper, we have used openQCD [44] for generating the configurations and applying the 4D gradient flow, and then implemented the calculation of (3.2) separately. We update with the HMC algorithm with trajectories of length 1.5 (in lattice units), measuring every 60 updates. The autocorrelation between configurations is then acceptable for the N_s values we use. For the statistical analysis we have used the Γ-method algorithm as provided in [45] as a Python module.

When integrating the 3D slices along the flow direction, we have also used blocking-techniques (as were described in [43]) after the energy had been lowered below a threshold (chosen such that the blocking did not change the final answer). It is also important to note that while the integration of the 4D gradient flow discretization needs to be done as precisely as possible (and for that, we have used the 3rd order Runge-Kutta algorithm already implemented in openQCD), the integration for the 3D slices can be done with a much simpler Euler algorithm with bigger step-size, as the most important part is that we end up in vacuum (where all links are close to unity), and not the precise configuration we pass through in the middle.

For the scale setting, we have used the fitting parameters found in [46, 47] which allows us to find the β_{latt} necessary to equilibrate our lattice to our desired temperature, given the number of sites in the time direction N_t. For reference, we have included in table 1 the value of the lattice coupling for different cases we have used in this work.

Before trying to understand the continuum limit of this method, and to be sure we are on the right track, we first test that the procedure really returns integer values of Q_S. We do this on a single lattice size and spacing and a single chosen value of 4D gradient flow depth and show the results in figure 7. We see that, while the individual components Q_0, Q_{half}, $Q_{\beta/2}$ are definitely not topological and take a range of values, the combination Q_S is indeed topological up to modest fluctuations caused by $\mathcal{O}(a^2)$ high-dimension operator contamination in our definition of topological density. This effect gets smaller as we apply more 4D gradient flow (see below). In practice we must apply enough 4D gradient flow to cleanly separate the different integer values, which can be checked by making a histogram of Q_S values and seeing that they separate into clear peaks. Then one assigns integer values by projecting to the closest integer. We illustrate how this works in figure 8, where we see

JHEP01(2023)155

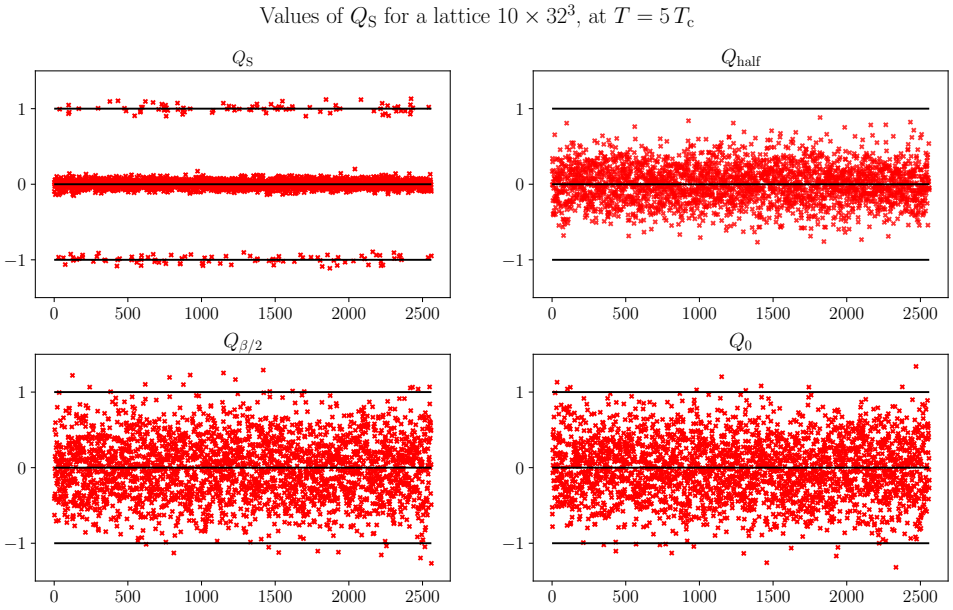

Figure 7. Numerical data obtained from 2560 configurations on a lattice with 10×32^3 sites, equilibrated at a temperature $T = 5\,T_c$, where the measurement has been performed at a gradient flow depth of $\tau_F = 1.2a^2$. The top-left plot is Q_S of each configuration, and is approximately an integer. The top-right, bottom-left, and bottom-right plots show the Q_{half}, Q_0, and $Q_{\beta/2}$, respectively.

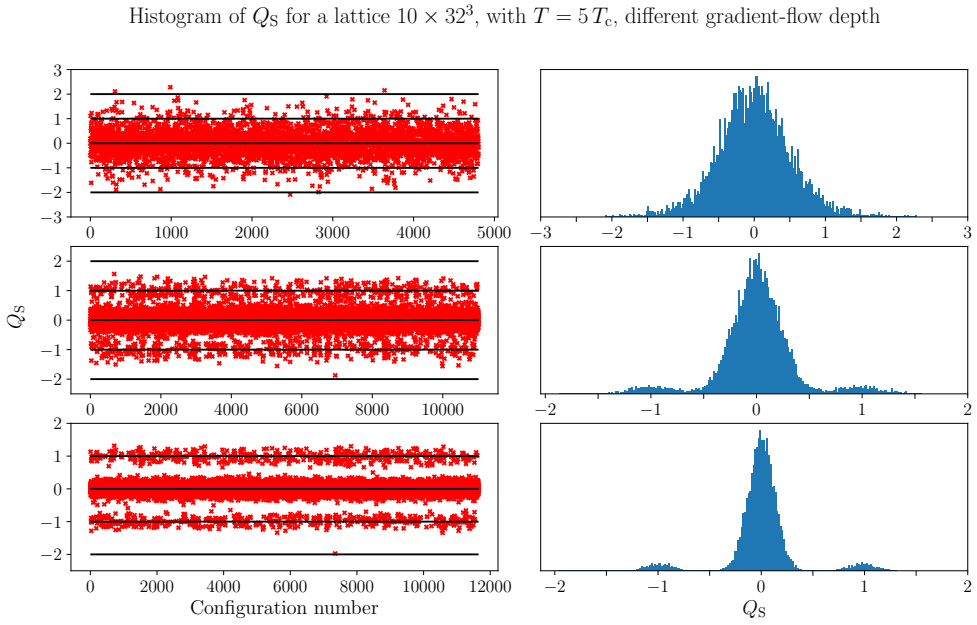

Figure 8. Histograms of Q_S for a lattice with 10×32^3 sites, at temperature $T = 5\,T_c$, and different gradient flow depths. The amount of flow corresponds to $\tau_F = [0.2, 0.4, 0.6]\,a^2$, top to bottom. We see that as we go down the flow path, the peaks are more defined. While for $\tau_F/a^2 = 0.2$ we cannot see the topological nature of the jumps, that becomes clear for $\tau_F/a^2 = 0.4$. As a remark, the criterion (4.3) fails for the top case, but is satisfied for the other two.

JHEP01(2023)155

the histogram of Q_S at different gradient flow depths, and precisely check that the peaks get sharper as we go down the flow path.

The quantitative criterion we use to determine whether enough 4D gradient flow has been used is the following. First, we consider all configurations with $|Q_S| < 0.5$ and we evaluate the standard deviation $\sigma^2_{\text{data}} = \langle Q_S^2 \rangle_{|Q_S|<0.5}$. Assuming that the true distribution is Gaussian, we ask how much of the distribution is expected to lie outside the range $|Q_S| < 0.5$, and we require that this be less than 2%:

$$\int_{1/2}^{\infty} \frac{2\mathrm{d}z}{\sqrt{2\pi\sigma^2_{\text{data}}}} e^{-\frac{z^2}{2\sigma^2_{\text{data}}}} = \operatorname{erfc}\left(\frac{1}{2\sqrt{2}\sigma_{\text{data}}}\right) < 0.02 \quad \rightarrow \quad \sigma_{\text{data}} < 0.215\,. \tag{4.3}$$

5 Volume, lattice spacing, and gradient-flow depth dependence

Now that we have formulated the theoretical framework of the calculation and shown that it works numerically, we need to analyze how it behaves on the lattice. The three main topics we should study are:

1. how to correct the rate for the effects of 4D gradient flow,
2. how it changes when we vary the spatial volume of our lattices, and
3. how to take the continuum limit, that is, how it changes when we go to finer lattices (by varying the number of sites in the time direction, and varying β_{latt} such that the temperature is constant).

5.1 Gradient flow dependence

As explained in the previous section, some 4D gradient flow is needed to ensure that Q_S is really topological up to fluctuations which are small enough to fix by projecting to the nearest integer. However, applying this gradient flow can move individual time-slices across the separatrix and reduces how many configurations are determined to be sphalerons. We have to correct for this effect. The analytical dependence in the case of a single degree of freedom has already been explored in section A.2, and here we will check that the same relationship holds for the case of QCD on the lattice. By taking the quotient between equations (A.13) and (A.20), we can find that

$$\frac{\Gamma^{\tau_F}_{\text{sphal},s}}{\Gamma_{\text{sphal},s}} = \frac{2}{\pi}\sqrt{2\sum_{\substack{n=1\\ n\text{ odd}}}^{\infty} \frac{e^{-\overline{\tau}_F n^2}}{n^2}} \tag{5.1}$$

where we have defined $\overline{\tau}_F \equiv 8\pi^2\tau_F/\left(a^2N_t^2\right)$.

We can then explore the accuracy of this correction by examining the same ensemble of configurations using different amounts of gradient flow. The result can be seen in figure 9, where the points in the left represent the sphaleron rate $\Gamma^{\tau_F}_{\text{sphal},s}$, while on the right they have been corrected according to (5.1). We see that, for gradient flow depths above a threshold of about $\tau_F = 0.5a^2$, the correction accurately describes the effect of gradient flow.

JHEP01(2023)155

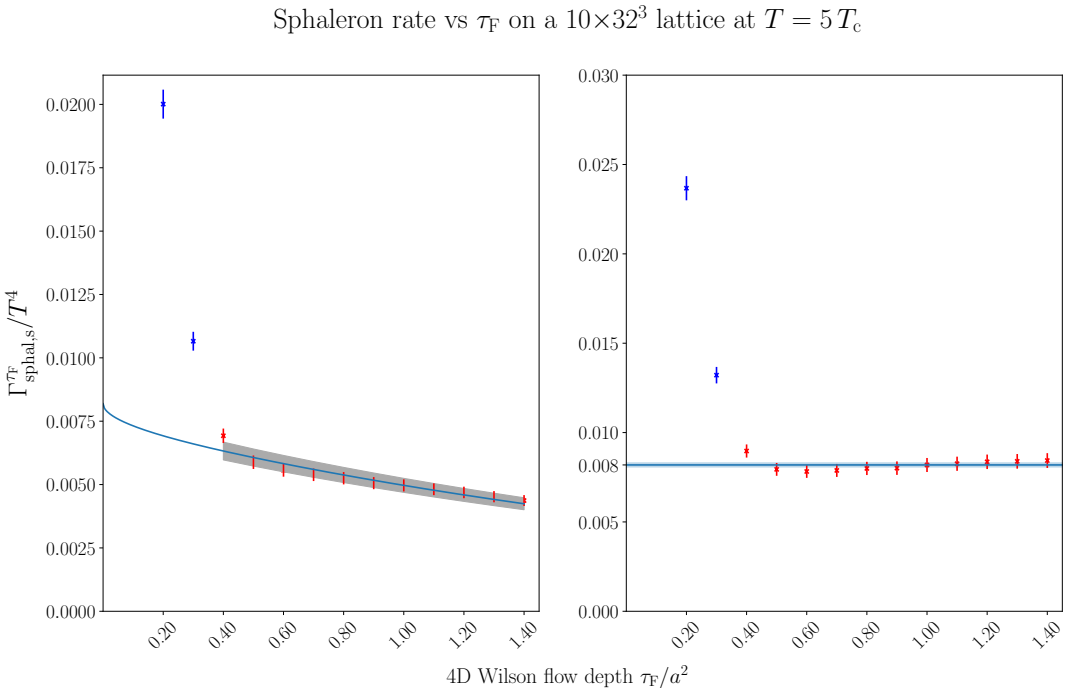

Figure 9. Left: measurement of the sphaleron rate at different gradient-flow depths, where the points in red (representing different values of $\Gamma^{\tau_F}_{\mathrm{sphal},s}$) have been used to find the best fit for $\Gamma_{\mathrm{sphal},s}$ (see equation (5.1)). The points in blue do not satisfy the criterion explained in a previous section, equation (4.3). Right: same plot but where each value has been corrected according to (5.1), and the horizontal line is the best fit described before. We see that the correction successfully accounts for the effects of 4D gradient flow.

We expect the correction to break down when τ_F comes of order β^2, that is, $a^2N_t^2$, when the gradient flow starts erasing all information stored in the gauge fields. We have not explored this regime in detail because we don't need to — as long as there is a range of τ_F values where the correction works well, then we can use this to establish the sphaleron rate in a τ_F-independent way. This should be possible whenever N_t is sufficiently large, which is the same as a requirement that the lattice spacing be sufficiently small.

5.2 Volume dependence

The sphaleron rate has been computed at very high temperatures (or weak gauge couplings) using classical-field, real-time methods, and it was always found that the rate per unit 4-volume is suppressed in small boxes but grows to an infinite-volume asymptotic value above some box size [30, 48, 49]. Intuitively, this means that sphalerons have a typical intrinsic size, and the box must be larger than this size for a sphaleron to "fit." At weak coupling, the size is expected to be parametrically of order $1/g^2T$ [7, 40]. In the 4D Euclidean calculation we expect something similar to happen: in lattices with N_t sites in the temporal direction and N_s sites in the spatial direction, for small N_s we will not observe any jumps. As we make the spatial volume bigger (keeping β_{latt} and N_t fixed), we will start observing more and more jumps. Eventually, we would expect $\langle Q_S^2\rangle/V$ to approach a constant.

JHEP01(2023)155

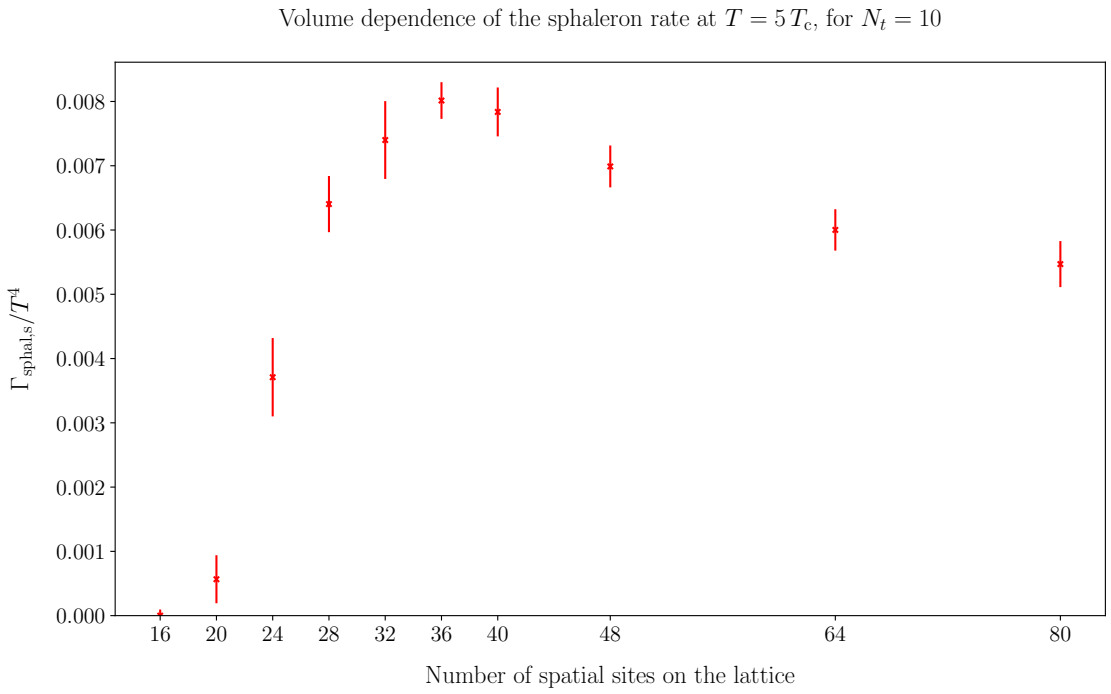

Figure 10. Sphaleron rate as a function of the aspect ratio N_s/N_t, at fixed N_t and temperature.

We can see the result for different values of N_s in figure 10, where we have used a lattice with $N_t = 10$ and equilibrated it at $T = 10\,T_c$. As expected, we see the increase in the sphaleron rate as we increase the volume until it reaches the peak. But from that point forward, we see a decrease in the rate. We did not expect this and it is not analogous to what occurs in the real-time case. To show this more clearly, we have revisited the volume dependence of the classical real-time SU(2) rate using the same code as in ref. [49]. Fixing the lattice spacing to $a = 0.25g^2T$ and varying the box size, figure 11 shows that the classical real-time rate saturates to a flat asymptotic value to within a few percent, without the clear post-peak decrease we observe in the Euclidean method.

We do not yet understand why our sphaleron-rate volume dependence exhibits a peak and a decrease towards very large volumes. Note that the configurations at larger volumes than the peak frequently exhibit $|Q_S| > 1$, which means that there are multiple sphalerons in a box or that our single-saddlepoint picture has broken down. Since it is unclear if our approach is really appropriate in this regime, we will use the peak in the volume-dependence curve as our sphaleron-rate estimate in the remainder of this work. Clearly it would be valuable to revisit this decision and to find a clearer understanding of the large-volume behavior and the meaning of this peak and falloff. We will assume that our results suffer an $\mathcal{O}(30\%)$ systematic uncertainty because of this assumption.

5.3 Continuum limit

Now the only thing we need to check is how $\Gamma_{\mathrm{sphal},s}$ approaches the continuum limit $a \to 0$ at fixed temperature and aspect ratio. We do this by performing the calculation at a series

JHEP01(2023)155

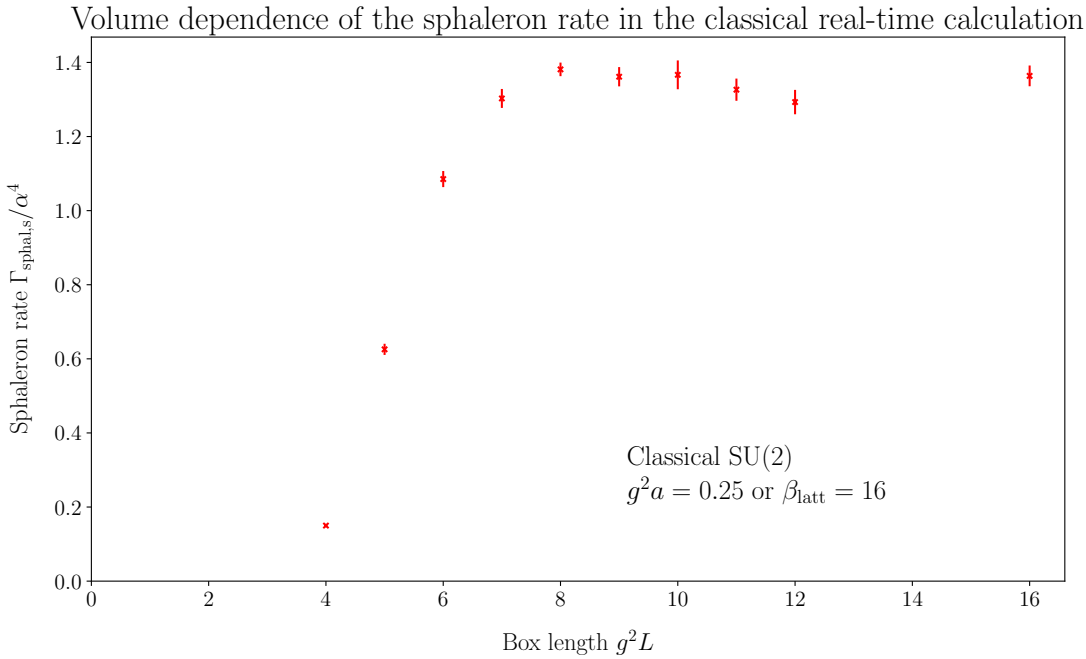

Figure 11. Volume dependence of the SU(2) sphaleron rate when the rate is determined using classical-field, real-time techniques as in ref. [49]. As the volume increases, the rate rises and saturates to a very clear plateau.

of lattice spacings (or N_t values) and seeing how they scale with a^2. As has been explained in section 4, we use the scale setting as described in [46, 47] in order to relate the lattice spacing a to the lattice coupling β. Then we can fix the temperature while increasing N_t and calculate the sphaleron rate at the peak in each case,[6] using the previously established method to correct for 4D gradient-flow effects.

The result can be seen in figure 12. As frequently happens, lattice spacing effects are large at $N_t = 6$, but for larger N_t we find a good convergence towards a continuum limit.

Rather than repeat this continuum limit procedure at every temperature, we will fix to $N_t = 10$ at all other temperatures, which we see will introduce at most $\sim 20\%$ errors in our results.

6 Low and high temperatures

Before we proceed to show the final results for the sphaleron rate at different temperatures, we also need to comment on the limits of our method.

6.1 Low temperatures and instantons

Consider the toy model one more time. In the high-temperature regime, the φ field typically reaches $\varphi = \pi$ as a result of a Euclidean history which loiters near $\varphi = \pi$ (a sphaleron),

[6] We also checked that the aspect ratio N_s/N_t where the rate reaches its peak is independent of lattice spacing.

JHEP01(2023)155

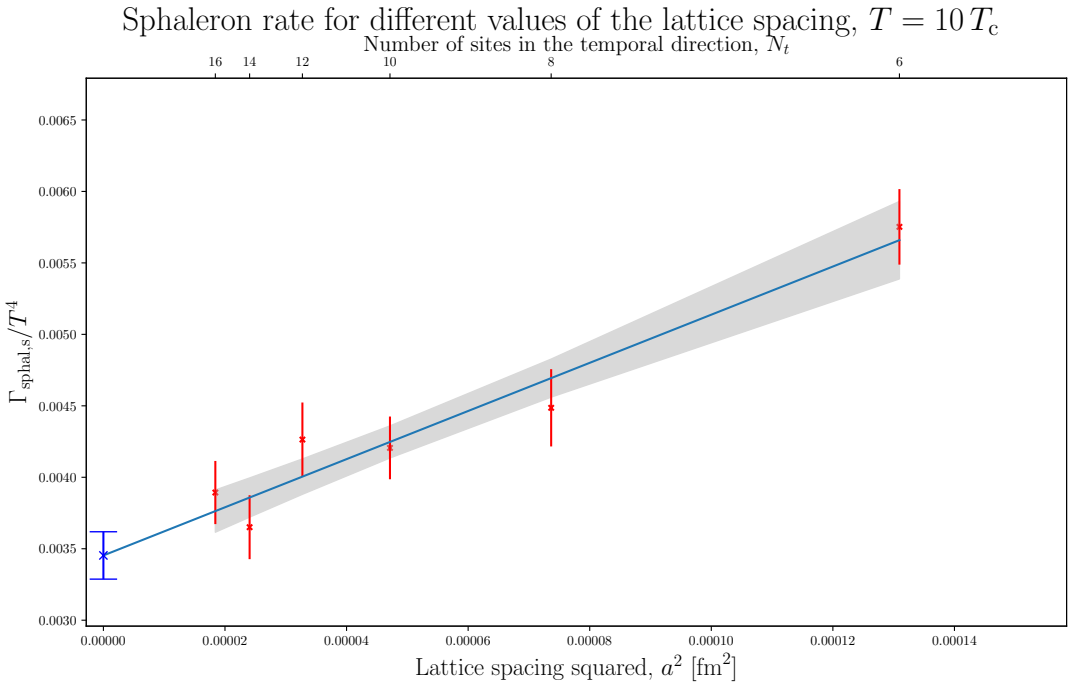

Figure 12. Sphaleron rate calculated at the peak of each volume-dependence curve, extrapolated to zero gradient-flow-depth, at different values of lattice spacing a, for $T = 10\,T_c$. The zero-spacing extrapolation yields a value of $\Gamma_{\mathrm{sphal},s}/T^4 = 0.0035 \pm 0.0002$.

rather than a history which transitions from $\varphi = 0$ to $\varphi = 2\pi$ (an instanton). But as the temperature is lowered, the instantons become more important. In this case, the basic picture — that the real-time rate is controlled by classical thermal fluctuations up to the barrier and the rate can be computed from the frequency of such transitions over the barrier — comes into question. Therefore we should not trust our approach if instantons are as common as sphalerons.

One feature of our approach, as one sees in figure 4 for instance, is that a sphaleron will give the same answer whether we include the Euclidean path between $t = 0$ and between $t = \beta/2$ as we would find if we include the Euclidean path between $t = \beta/2$ and $t = \beta$. We see this more explicitly in eq. (3.3). If we had chosen $t = \beta/2$ and $t = \beta$ as the lower and upper boundaries of our region, we would define

$$\begin{aligned} Q'_{\mathrm{S}} &= Q(t = \beta/2) + \left[\int_{\beta/2}^{\beta} \mathrm{d}t \int \mathrm{d}^3x\, q(x,t)\right] - Q(t = \beta) \\ &= Q_{\beta/2} + Q_{\mathrm{second-half}} - Q_0 \\ &= -(Q_0 + Q_{\mathrm{half}} - Q_{\beta/2}) + \left[\int_{0}^{\beta} \mathrm{d}t \int \mathrm{d}^3x\, q(x,t)\right] \\ &= -Q_{\mathrm{S}} + Q_{\mathrm{I}}\,. \end{aligned} \tag{6.1}$$

In passing from the first to second line we use periodicity, which means that the configuration at $t = \beta$ is the same as at $t = 0$ so $Q_\beta = Q_0$. The integral on the third line is the total

JHEP01(2023)155

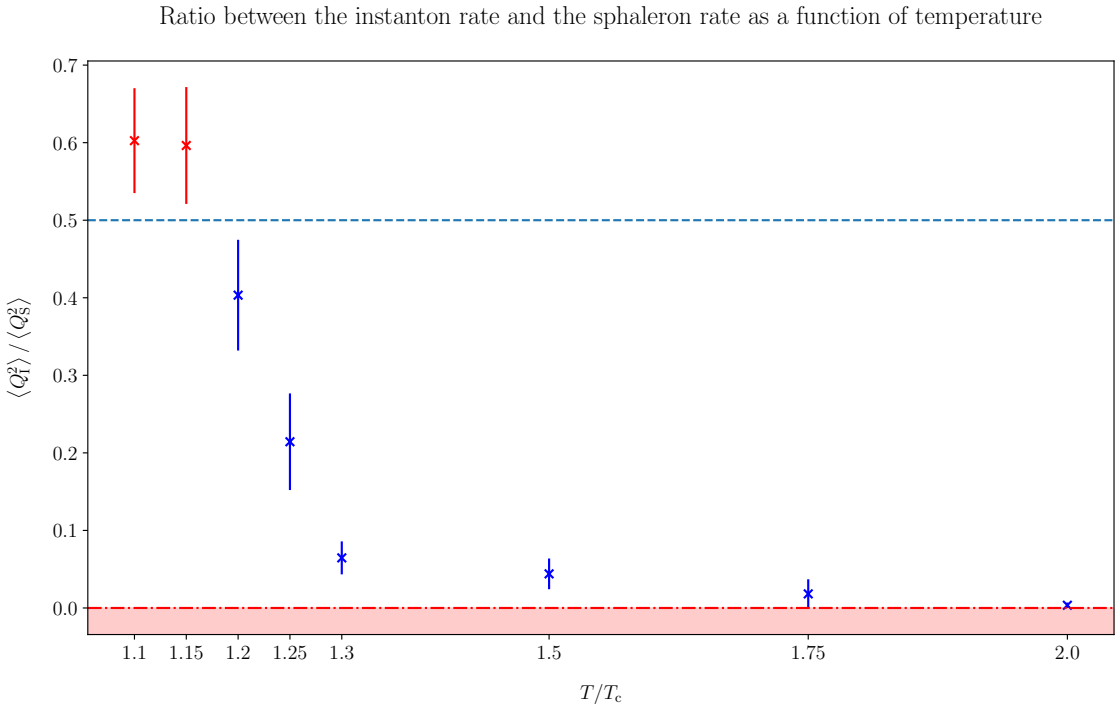

Figure 13. Ratio between the amount of instantons ($Q_I \neq 0$) and sphalerons ($Q_S \neq 0$) as a function of temperature (in T_c units). Only the sphaleron rate has been extrapolated to zero gradient-flow-depth, as described in the previous section.

topology in the box, Q_I. At high temperatures Q_I is almost always zero, and therefore $Q'_S = -Q_S$; the topology we find in the upper half of the box is minus the topology we find in the lower half. But for configurations with an actual instanton, $Q_I = \pm 1 = Q_S + Q'_S$. Therefore, true sphalerons ($Q_S = \pm 1$ but $Q_I = 0$) will count as a sphaleron whether we use the top or the bottom half of our box, whereas instantons will *either* count as a sphaleron if we use the top half, *or* if we use the bottom half.

As we just emphasized, the whole approach of counting sphalerons and equating them to classical transitions becomes suspect when a large fraction of what we find are actually instantons. Therefore it is useful to investigate the ratio of the instanton density to the sphaleron rate. When this ratio becomes of order 1/2, we have left the regime where classical activation makes sense. When the ratio is small, sphalerons dominate instantons and our approach should make sense.

We present this comparison in figure 13. For values of temperatures above $1.75\,T_c$ the appearance of instantons is exponentially suppressed and finding one is very rare. For values between 1.3 and $1.75\,T_c$, while we can find some instantons, they are rare when compared to the amount of sphalerons (sphalerons are at least 10 times more common than instantons). For values lower than $1.3\,T_c$, the instantons are very common and therefore we cannot trust our calculation for the sphaleron rate. Therefore, our method will only be reliable above $1.3\,T_c$, and we will restrict ourselves to this domain.

JHEP01(2023)155

6.2 High temperatures and classical fields

At very high temperatures the gauge coupling becomes so weak that $g^2 T \ll T$. In this case, sphalerons are physically large objects which should be well described in terms of classical fields, both thermodynamically and (within limits) dynamically. In this regime, both our methods and previous, classical-field real-time methods should be applicable. Therefore we will attempt to make contact with the 3D real-time results of ref. [30].

Real-time results are calculated in terms of the effective 3D gauge coupling g_3^2, which equals $g^2 T$ of the 4D theory at tree level. At the loop level, it can be related to the 4D $\overline{\text{MS}}$ coupling via a perturbative matching calculation, which has been carried out to 2 loops by Laine and Schroeder in ref. [50], see eq. (2.34) to (2.37) of that reference.

The $\overline{\text{MS}}$ coupling can in turn can be related to the lattice coupling β_{latt} by measuring the gradient-flowed expectation value of the squared field strength $E \equiv \text{Tr}\, G_{\mu\nu} G^{\mu\nu}$ and using its NNLO relation to the $\overline{\text{MS}}$ coupling at $\mu = 1/\sqrt{8\tau_{\text{F}}}$ [51]:

$$t^2 \langle E(t) \rangle = \frac{3\alpha_s}{4\pi} \left(1 + k_1 \alpha_s + k_2 \alpha_s^2\right) \tag{6.2}$$

where $k_1 \approx 1.098$ and $k_2 \approx -0.982$ for SU(3) theory without fermions. We use the Wilson action, Zeuthen flow [52], and clover definition of the field strength, checking that the result is stable over a range of flow depths after the 2-loop running of $g^2(\mu_{\overline{\text{MS}}})$ is taken into account.

Equipped with this method, we study a lattice with $N_t = 8$ and $\beta_{\text{latt}} = 15$, finding that it corresponds to $\frac{g_3^2}{4\pi} = 0.0406$. Since the coupling is small, the box size must be correspondingly large before the sphaleron rate "turns on." For this choice of N_t, we find that we need $N_s = 96$ to reach the peak in the volume dependence of the sphaleron rate. Generating many independent configurations of this size is challenging, so our statistical errors are rather large; we find that $\Gamma^{\text{new}}_{\text{sphal},s}/(\alpha_s^4 T^4) = 19 \pm 7$. Based on figure 12, we expect the real answer to be 20% to 25% lower once the continuum limit is performed. Going back to [30], we find that for $\alpha_s(0 \text{ flavor}) = 0.039$, the value is $\Gamma^{\text{old}}_{\text{sphal},s}/(\alpha_s^4 T^4) = 11.5 \pm 0.3$. Therefore, our method is compatible with the previous 3D calculations, given the downwards continuum corrections, the rather large statistical errors, and the theoretical errors present in the calculation in [30].

7 Results, discussion, and conclusions

The results obtained with our method for the sphaleron rate in the range of temperatures $[1.3{-}20]\, T_{\text{c}}$ are shown in figure 14 and summarized in table 2. We emphasize that these results are at $N_t = 10$; we have not taken a continuum limit.

The main application of these rates is to use them in eq. (1.4) to see how quickly or slowly a chiral imbalance relaxes via thermal sphaleron processes. Using $\Gamma_{\text{sphal},s}/T^3 \simeq 0.04T$ over the range $[1.3T_{\text{pc}}, 2T_{\text{pc}}]$ and treating the up and down flavors as light ($n_f = 2$), we estimate that the exponential decay lifetime for axial number is of order $12/T$. This is slow enough to allow axial number to play a role in early dynamics during heavy ion collisions, but marginally fast enough for axial number to relax before the system

JHEP01(2023)155

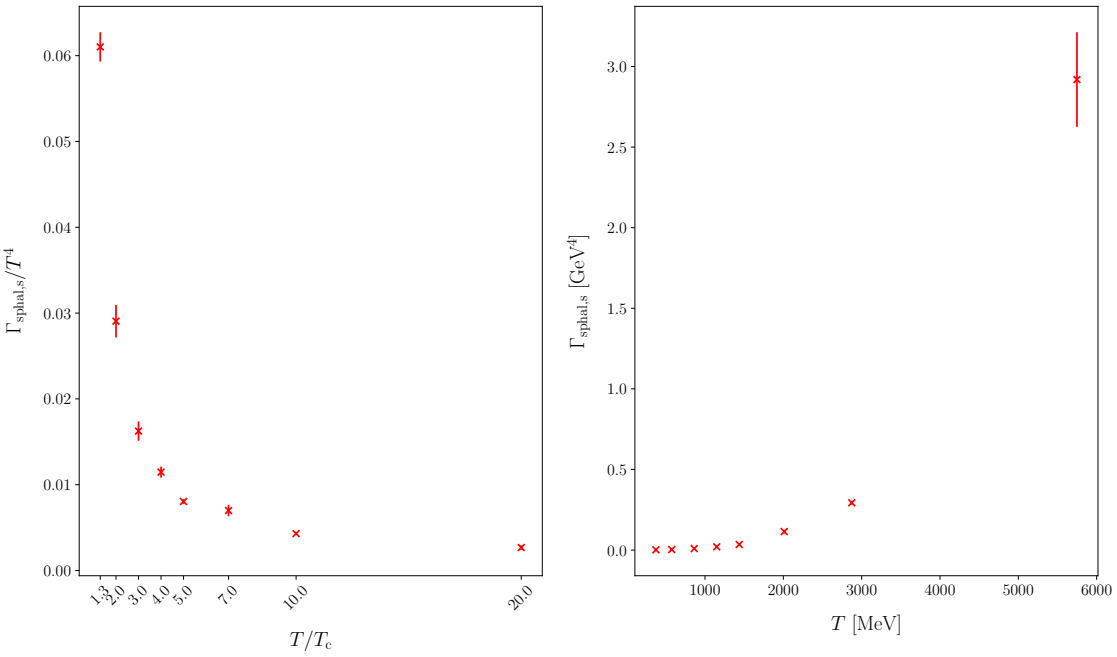

Figure 14. Results for the sphaleron rate for different temperatures. The left plot presents the dimensionless ratio found by scaling with T^4, while on the right we have reintroduced dimensions, using $T_c \approx 280\,\mathrm{MeV}$ for SU(3) theory. Errors are statistical only; all data are at $N_t = 10$ without a continuum extrapolation.

T/T_c	$\Gamma_{\mathrm{sphal},s}/T^4$	$\Gamma_{\mathrm{sphal},s}$ [GeV^4]	Num. configs.
1.3	0.061 ± 0.002	0.00119 ± 0.00003	5520
2.0	0.029 ± 0.002	0.0031 ± 0.0002	1970
3.0	0.016 ± 0.001	0.0089 ± 0.0006	1280
4.0	0.0115 ± 0.0006	0.020 ± 0.001	2260
5.0	0.0080 ± 0.0003	0.034 ± 0.001	7680
7.0	0.0069 ± 0.0007	0.11 ± 0.01	1280
10.0	0.0043 ± 0.0002	0.29 ± 0.01	4560
20.0	0.0027 ± 0.0003	2.9 ± 0.3	1280

Table 2. Results presented in figure 14 in tabular form. Errors are statistical only.

hadronizes. Note that this estimate involves using pure-glue results in full QCD, and it therefore still has rather large theory errors.

We have also calculated the sphaleron rate at the electroweak scale, where the coupling is approximately $\alpha_s \sim 0.1$. For that we have used the same techniques as in section 6.2 to find the 4D coupling from gradient flow. For $\beta_{\mathrm{latt}} = 9$, we have found that it corresponds to $\alpha_s = 0.108 \pm 0.002$ (where the uncertainty shown is not statistical but comes from having to pick a flow depth such that equation (6.2) is valid but lattice errors are small). In this

JHEP01(2023)155

case, we obtain

$$\Gamma_{\mathrm{sphal},s}(\alpha_s \sim 0.108) = 14 \pm 1\, \alpha_s^4 T^4. \tag{7.1}$$

We emphasize again that the error is statistical only; we have not taken a continuum limit and that the result is for pure glue, so there are still much larger systematic effects to be included.

The main breakthrough of this paper is to show how real-time processes mediated by semiclassical saddlepoints, like thermal bubble nucleation or the sphaleron rate, can be calculated using exclusively Euclidean and fully nonperturbative tools. We have applied this technique to the sphaleron rate in SU(3) gauge theory partly because of its phenomenological interest and partly because it is particularly clear in this case how to define the separatrix and how to determine whether the $t = 0$ and $t = \beta/2$ time slices of the Euclidean path integral lie on opposite sides of the separatrix. The same approach should be applicable to other saddle-controlled tunneling processes such as bubble nucleation, though identifying the saddlepoint in this case may be more challenging. Our approach also has the weakness that it does not give us a way to determine a dynamical prefactor $\mathbf{d}$ which appears in the tunneling rate. Note that this same defect is present in analytical Euclidean approaches such as Affleck's method as well. We currently don't see a way to overcome this limitation.

It should be straightforward to extend the current approach to full QCD with 2+1 light flavors of fermions. The only change needed is to include the fermions when performing the HMC lattice updates, so that the configurations are drawn from the full, rather than pure-glue, lattice ensemble. We have already begun work on this project.

There are a few points where it would be useful to deepen our understanding of the technique and our results. The unexpected scaling with lattice volume needs to be better understood. And it would also be interesting to better understand lower temperatures where instantons start to play a role. To what extent can we incorporate instantons into a determination of axial number relaxation? And to what extent does axial quark number make sense in a regime where the system is moving towards a description in terms of hadronic degrees of freedom? We consider these to be interesting open issues.

Acknowledgments

The authors acknowledge support by the Deutsche Forschungsgemeinschaft (DFG, German Research Foundation) through the CRC-TR 211 'Strong-interaction matter under extreme conditions' – project number 315477589 – TRR 211. Calculations were performed on the high-performance computer Lichtenberg at the NHR Centers NHR4CES at TU Darmstadt.

A Size of Euclidean fluctuations

We have argued that the sphaleron rate can be determined by finding which Euclidean configurations "span" the separatrix, in the sense that the spatial slice at $t = 0$ and the slice at $t = \beta/2$ are on different sides of the separatrix.

JHEP01(2023)155

Here we present the details of the calculation comparing the likelihood for a Euclidean configuration to satisfy this condition to the real-time rate for transitions as determined by the Affleck method. We also incorporate the effect of 4D gradient flow applied to the Euclidean configuration before the measurements are carried out.

The main assumption behind the method is that the sphaleron, critical bubble, or other object responsible for tunneling is a robust high-action object. Even though the transition rate may not be dominated by configurations close to the saddle point, it will be dominated by configurations in the vicinity of the (codimension-1) separatrix surface. At every point on the separatrix there is a direction orthogonal to the separatrix, and we assume that fluctuations along this direction, when comparing 3D slices at different t values, are small relative to the overall size of the sphaleron. In this case the degree of freedom $\phi(t)$ associated with this direction can be treated as a single variable with a kinetic term whose strength is approximately ϕ-independent and a potential which can be approximated as quadratic. (We do *not* need this kinetic term or this potential to be the same everywhere on the separatrix — we only need to know that there is little variation orthogonal to the separatrix, over the field-space distances explored by the higher Matsubara modes of this degree of freedom.) If these assumptions are far from correct, the entire saddlepoint approach we use will not be applicable and we have no theoretical tools to establish the rate from Euclidean methods (and probably real-time methods will also not be applicable since they also rely on a scale separation between the size and evolution time scale of sphalerons and the intrinsic thermal size and time scales).

A.1 Calculation without gradient flow

We are interested in a configuration close to some point on a separatrix surface, and in the degree of freedom orthogonal to the separatrix. We will write this degree of freedom as $\phi(t)$ with $\phi = 0$ representing the separatrix, and we take it to have a canonically normalized kinetic term (recall that a rescaling of $\phi(t)$ does not affect our answers). For the toy model, $\phi(t) = \sqrt{m}(\varphi(t) - \pi)$. The probability that the Euclidean fluctuations carry ϕ across $\phi = 0$ between $t = 0$ and $t = \beta/2$ are given by:

$$\Gamma_{\rm Eucl} \equiv \int_{\phi(t=0)=\phi(t=\beta)} \mathcal{D}\phi\, e^{-S_E} \left[\theta(\phi(t{=}0))\theta(-\phi(t{=}\beta/2)) + \theta(-\phi(t{=}0))\theta(\phi(t{=}\beta/2))\right]. \tag{A.1}$$

The two $\theta(..)\theta(..)$ factors represent cases where ϕ goes from positive to negative and where it goes from negative to positive, respectively. Here the Euclidean action S_E is

$$S_E = \int_0^\beta {\rm d}t \left(\frac{1}{2}\left(\partial_t\phi\right)^2 - \frac{m^2}{2}\phi^2\right), \tag{A.2}$$

with m^2 representing a possible potential, favoring ϕ to leave the separatrix (the curvature in the unstable direction of the saddlepoint). We insert the following Matsubara decomposition, which satisfies the periodicity condition but is otherwise general:

$$\phi(t) = \phi_0 + \sum_{n=1}^{\infty} \left(c_n \cos(2\pi n t/\beta) + s_n \sin(2\pi n t/\beta)\right). \tag{A.3}$$

JHEP01(2023)155

With this substitution, the measure of the path integral becomes simply

$$\mathcal{D}\phi = \mathcal{N} \mathrm{d}\phi_0 \prod_{k=1}^{\infty} \mathrm{d}c_k \mathrm{d}s_k \tag{A.4}$$

where $\mathcal{N}$ is a constant, and we can explicitly evaluate the action

$$\begin{aligned} S_E &= -\frac{\beta\, m^2}{2}\phi_0^2 + \sum_{n=1}^{\infty}(c_n^2 + s_n^2)A(n,m)\,, \\ A(n,m) &\equiv \frac{\beta}{4}\left[\left(\frac{2\pi n}{\beta}\right)^2 - m^2\right]. \end{aligned} \tag{A.5}$$

Introducing c_{even} and c_{odd} as the sum over the even and odd c_k coefficients through

$$1 = \int \mathrm{d}c_{\text{even}}\, \mathrm{d}c_{\text{odd}}\; \delta\left(c_{\text{even}} - \sum_{k=2,4,\ldots} c_k\right) \delta\left(c_{\text{odd}} - \sum_{k=1,3,\ldots} c_k\right) \tag{A.6}$$

we can rewrite the Heaviside theta-functions as:

$$\begin{aligned} \theta(\phi(t=0)) &= \theta\left(\phi_0 + \sum_k c_k\right) = \theta(\phi_0 + c_{\text{even}} + c_{\text{odd}})\,, \\ \theta(-\phi(t=\beta/2)) &= \theta\left(-\phi_0 - \sum_k (-1)^k c_k\right) = \theta(-\phi_0 + c_{\text{even}} - c_{\text{odd}})\,. \end{aligned} \tag{A.7}$$

so that the path integral we have to perform is given by

$$\begin{aligned} \Gamma_{\text{Eucl}} = 2\int \mathrm{d}\phi_0 \int \mathrm{d}c_{\text{even}} \mathrm{d}c_{\text{odd}} \prod_{k=1}^{\infty} \mathrm{d}c_k \mathrm{d}s_k \, \exp\left(\frac{m^2}{2}\phi_0^2\beta - \sum_{n=1}^{\infty}(c_n^2 + s_n^2)A(n,m)\right) \\ \times\, \delta\left(c_{\text{even}} - \sum_{k=2,4,\ldots} c_k\right) \delta\left(c_{\text{odd}} - \sum_{k=1,3,\ldots} c_k\right) \theta(\phi_0 + c_{\text{even}} + c_{\text{odd}})\theta(-\phi_0 + c_{\text{even}} - c_{\text{odd}}). \end{aligned} \tag{A.8}$$

The factor of 2 accounts for the other θ-function combination, which gives precisely the same answer as the one shown.

Exponentiating the delta functions

$$\delta\left(c_{\text{even}} - \sum_k c_k\right) = \int \frac{\mathrm{d}\lambda}{2\pi}\, \exp\left(i\lambda c_{\text{even}} - i\sum_k \lambda c_k\right) \tag{A.9}$$

makes all integrals either Gaussians or modified Gaussians, and it is straightforward to evaluate them.

This calculation suffers from an unknown overall scaling, but recall that we are interested in the ratio of this result to the standard result, which is $\langle|\mathrm{d}\phi/\mathrm{d}t_{\mathrm{m}}|\rangle$ times the probability density for $\phi_0 = 0$. Equipartition tells us that $\langle|\mathrm{d}\phi/\mathrm{d}t_{\mathrm{m}}|\rangle = \sqrt{\frac{2T}{\pi}}$, see eq. (2.5). To evaluate the probability density, we compute the same path integral, but with the two Heaviside functions replaced by a single delta function $\delta(\phi_0)$ — essentially, this determines the normalization factor $\mathcal{N}$:

$$\mathcal{N} = \int_{\phi(t=0)=\phi(t=\beta)} \mathcal{D}\phi \exp\left(-\int_0^{\beta} \mathrm{d}t \frac{1}{2}\left(\partial_t\phi\right)^2\right)\delta(\phi_0)\,, \tag{A.10}$$

JHEP01(2023)155

which means that

$$\mathcal{N} = \prod_{n=1}^{\infty} \frac{A(n,0)}{\pi}. \tag{A.11}$$

With this, by defining

$$\begin{cases} S_{\text{odd (even)}} & \equiv \displaystyle\sum_{n\,\text{odd (even)}} \frac{1}{4A(n,m)} \\ C & \equiv \dfrac{1}{4S_{\text{even}}} - \dfrac{m^2\beta}{2} \\ b & \equiv \dfrac{m^2\beta}{2}\left(1 + \dfrac{m^2\beta}{8C}\right) \end{cases} \tag{A.12}$$

the final result for the integral (A.1) is

$$\Gamma_{\text{Eucl}} = e^{-\frac{m^2\beta}{2}} \frac{m\beta}{2\sin(m\beta/2)} \sqrt{\frac{1}{\pi S_{\text{even}} b C}} \operatorname{arctanh}\left(2\sqrt{S_{\text{odd}} b}\right). \tag{A.13}$$

When the saddlepoint is a strongly semiclassical configuration, the action should not change too quickly as we move away from it, meaning that $m/2\pi T \ll 1$. If we expand the result in this limit, it simplifies:

$$\Gamma_{\text{Eucl}} = 4e^{-m^2\beta/2}\sqrt{\frac{S_{\text{odd}}}{\pi}} + \mathcal{O}\left(\sqrt{\beta}(m\beta)^2\right) = \sqrt{\frac{\beta}{2\pi}} + \mathcal{O}\left(\sqrt{\beta}(m\beta)^2\right). \tag{A.14}$$

This is the rate divided by the probability density to be on the separatrix. To fully normalize it by the real-time rate, we should divide by $\sqrt{2T/\pi}$ which we found above, to find:

$$\frac{\Gamma_{\text{Eucl}}}{\text{real-time rate}} = \sqrt{\frac{1}{2\pi T}}\left(\sqrt{\frac{2T}{\pi}}\right)^{-1} = \frac{1}{2T}, \qquad \text{or}$$

$$\text{Real-time rate} = 2T\,\Gamma_{\text{Eucl}}. \tag{A.15}$$

This provides the desired relation between the Affleck real-time rate and the Euclidean sphaleron density which we have defined.

A.2 Calculation with flow

In practice it is necessary to modify the $\phi(t)$ field inside the Euclidean path integral through the application of gradient flow, before performing any evaluations on it. How does this affect the probability that $\phi(t=0)$ and $\phi(t=\beta/2)$ are on opposite sides of the separatrix? We will answer this now. Gradient flow changes the measurables, not the path integral or path integral variables. In our case, it damps the t-dependent fluctuations through application of the heat equation. Define the depth of heat-equation flow to be τ_{F}. Then we set the $\tau_{\text{F}} = 0$ boundary conditions to be $\phi(\tau_{\text{F}} = 0, t) = \phi(t)$, and the gradient flow itself is described by

$$\partial_{\tau_{\text{F}}}\phi(\tau_{\text{F}}, t) - \partial_t^2\phi(\tau_{\text{F}}, t) = 0. \tag{A.16}$$

JHEP01(2023)155

Using the same Fourier-series expansion for $\phi(t)$ as before, one easily finds that

$$\phi(\tau_{\rm F}, t) = \phi_0 + \sum_{n=1}^{\infty} \left(c_n \cos(2\pi n t/\beta) + s_n \sin(2\pi n t/\beta)\right) \exp\Big(-\tau_{\rm F}\,(2\pi n/\beta)^2\Big). \tag{A.17}$$

Now we can proceed as we did in the unflowed case, but taking the flow into account on our theta functions, while the action remains the same as in (A.5). The Heaviside functions become

$$\begin{aligned} \theta(\phi(\tau_{\rm F}, 0)) &= \theta\left(\phi_0 + \sum_k c_k \exp\Big(-\tau_{\rm F}\,(2\pi n/\beta)^2\Big)\right) \\ \theta(-\phi(\tau_{\rm F}, \beta/2)) &= \theta\left(-\phi_0 - \sum_k (-1)^k\, c_k \exp\Big(-\tau_{\rm F}\,(2\pi n/\beta)^2\Big)\right). \end{aligned} \tag{A.18}$$

Proceeding as we have done before, and defining in this case

$$S^{\tau_{\rm F}}_{\text{odd (even)}} \equiv \sum_{n\,\text{odd (even)}} \frac{\exp\left(-2\tau_{\rm F}\,(2\pi n/\beta)^2\right)}{4A(n,m)} \tag{A.19}$$

we find

$$\begin{aligned} \Gamma^{\tau_{\rm F}}_{\rm Eucl} &= e^{-\frac{m^2}{2}\beta} \frac{m\beta}{2\sin(m\beta/2)} \sqrt{\frac{1}{\pi S^{\tau_{\rm F}}_{\rm even} bC}}\, \operatorname{arctanh}\left(2\sqrt{S^{\tau_{\rm F}}_{\rm odd} b}\right) \\ &\Rightarrow \sqrt{\frac{\beta}{2\pi}} \sqrt{\frac{8}{\pi^2} \sum_{n=1,3,\ldots} \frac{e^{-8\pi^2 \tau_{\rm F} T^2 n^2}}{n^2}} \\ &\simeq \sqrt{\frac{\beta}{2\pi}} \times \sqrt{1 - 8\sqrt{\frac{2\tau_{\rm F}}{\pi\beta^2}}}. \end{aligned} \tag{A.20}$$

As before, the quantity after $\Rightarrow$ is the result when taking $m \to 0$. The last line is the result of a small $\tau_{\rm F}$ expansion, with errors which are exponentially small provided that $\tau_{\rm F} \ll 1/(8\pi^2 T^2)$. In practice we will use the unexpanded expression shown in the middle line. The final expression is useful because it shows that the correction goes to 1 as $\tau_{\rm F} \to 0$ but only as a square root, that the behavior is monotonic, and that the domain over which the gradient flow can be viewed as "small" is roughly $\tau_{\rm F} \ll 1/(8\pi^2 T^2)$.

The best way to use this result is:

$$\text{Real-time rate} = \frac{2T\,\Gamma^{\tau_{\rm F}}_{\rm Eucl}}{\sqrt{1 - 8\sqrt{\frac{2\tau_{\rm F} T^2}{\pi}}}}\,. \tag{A.21}$$

JHEP01(2023)155

References

[1] A.A. Belavin, A.M. Polyakov, A.S. Schwartz and Y.S. Tyupkin, *Pseudoparticle Solutions of the Yang-Mills Equations*, *Phys. Lett. B* **59** (1975) 85 [INSPIRE].

[2] G. 't Hooft, *Symmetry Breaking Through Bell-Jackiw Anomalies*, *Phys. Rev. Lett.* **37** (1976) 8 [INSPIRE].

[3] G. 't Hooft, *Computation of the Quantum Effects Due to a Four-Dimensional Pseudoparticle*, *Phys. Rev. D* **14** (1976) 3432 [*Erratum ibid.* **18** (1978) 2199] [INSPIRE].

[4] S.L. Adler, *Axial vector vertex in spinor electrodynamics*, *Phys. Rev.* **177** (1969) 2426 [INSPIRE].

[5] J.S. Bell and R. Jackiw, *A PCAC puzzle: $\pi^0 \to \gamma\gamma$ in the σ model*, *Nuovo Cim. A* **60** (1969) 47 [INSPIRE].

[6] F.R. Klinkhamer and N.S. Manton, *A Saddle Point Solution in the Weinberg-Salam Theory*, *Phys. Rev. D* **30** (1984) 2212 [INSPIRE].

[7] V.A. Kuzmin, V.A. Rubakov and M.E. Shaposhnikov, *On the Anomalous Electroweak Baryon Number Nonconservation in the Early Universe*, *Phys. Lett. B* **155** (1985) 36 [INSPIRE].

[8] V.A. Rubakov and M.E. Shaposhnikov, *Electroweak baryon number nonconservation in the early universe and in high-energy collisions*, *Usp. Fiz. Nauk* **166** (1996) 493 [hep-ph/9603208] [INSPIRE].

[9] J.M. Cline, *Baryogenesis*, in *Les Houches Summer School - Session 86: Particle Physics and Cosmology: The Fabric of Spacetime*, Les Houches, France (2006).

[10] L.D. McLerran, E. Mottola and M.E. Shaposhnikov, *Sphalerons and Axion Dynamics in High Temperature QCD*, *Phys. Rev. D* **43** (1991) 2027 [INSPIRE].

[11] G.F. Giudice and M.E. Shaposhnikov, *Strong sphalerons and electroweak baryogenesis*, *Phys. Lett. B* **326** (1994) 118 [hep-ph/9311367] [INSPIRE].

[12] K. Fukushima, D.E. Kharzeev and H.J. Warringa, *The Chiral Magnetic Effect*, *Phys. Rev. D* **78** (2008) 074033 [arXiv:0808.3382] [INSPIRE].

[13] D.T. Son and P. Surowka, *Hydrodynamics with Triangle Anomalies*, *Phys. Rev. Lett.* **103** (2009) 191601 [arXiv:0906.5044] [INSPIRE].

[14] M.A. Stephanov and Y. Yin, *Chiral Kinetic Theory*, *Phys. Rev. Lett.* **109** (2012) 162001 [arXiv:1207.0747] [INSPIRE].

[15] A. Bazavov et al., *Quark number susceptibilities at high temperatures*, *Phys. Rev. D* **88** (2013) 094021 [arXiv:1309.2317] [INSPIRE].

[16] S. Borsányi, Z. Fodor, C. Hölbling, S.D. Katz, S. Krieg and K.K. Szabo, *Full result for the QCD equation of state with $2+1$ flavors*, *Phys. Lett. B* **730** (2014) 99 [arXiv:1309.5258] [INSPIRE].

[17] HotQCD collaboration, *Equation of state in $(2+1)$-flavor QCD*, *Phys. Rev. D* **90** (2014) 094503 [arXiv:1407.6387] [INSPIRE].

[18] D.Y. Grigoriev and V.A. Rubakov, *Soliton Pair Creation at Finite Temperatures. Numerical Study in (1+1)-dimensions*, *Nucl. Phys. B* **299** (1988) 67 [INSPIRE].

[19] D. Bödeker, L.D. McLerran and A.V. Smilga, *Really computing nonperturbative real time correlation functions*, *Phys. Rev. D* **52** (1995) 4675 [hep-th/9504123] [INSPIRE].

JHEP01(2023)155

[20] P.B. Arnold, D. Son and L.G. Yaffe, *The Hot baryon violation rate is $O(\alpha_w^5 T^4)$*, *Phys. Rev. D* **55** (1997) 6264 [hep-ph/9609481] [INSPIRE].

[21] D. Bödeker, G.D. Moore and K. Rummukainen, *Chern-Simons number diffusion and hard thermal loops on the lattice*, *Phys. Rev. D* **61** (2000) 056003 [hep-ph/9907545] [INSPIRE].

[22] J. Ambjørn, T. Askgaard, H. Porter and M.E. Shaposhnikov, *Sphaleron transitions and baryon asymmetry: A Numerical real time analysis*, *Nucl. Phys. B* **353** (1991) 346 [INSPIRE].

[23] J. Ambjørn and A. Krasnitz, *Improved determination of the classical sphaleron transition rate*, *Nucl. Phys. B* **506** (1997) 387 [hep-ph/9705380] [INSPIRE].

[24] G.D. Moore, C.-r. Hu and B. Müller, *Chern-Simons number diffusion with hard thermal loops*, *Phys. Rev. D* **58** (1998) 045001 [hep-ph/9710436] [INSPIRE].

[25] P.B. Arnold, *Hot B violation, the lattice, and hard thermal loops*, *Phys. Rev. D* **55** (1997) 7781 [hep-ph/9701393] [INSPIRE].

[26] D. Bödeker, *On the effective dynamics of soft nonAbelian gauge fields at finite temperature*, *Phys. Lett. B* **426** (1998) 351 [hep-ph/9801430] [INSPIRE].

[27] G.D. Moore, *The Sphaleron rate: Bodeker's leading log*, *Nucl. Phys. B* **568** (2000) 367 [hep-ph/9810313] [INSPIRE].

[28] P.B. Arnold and L.G. Yaffe, *High temperature color conductivity at next-to-leading log order*, *Phys. Rev. D* **62** (2000) 125014 [hep-ph/9912306] [INSPIRE].

[29] G.D. Moore, *Computing the strong sphaleron rate*, *Phys. Lett. B* **412** (1997) 359 [hep-ph/9705248] [INSPIRE].

[30] G.D. Moore and M. Tassler, *The Sphaleron Rate in* SU(N) *Gauge Theory*, *JHEP* **02** (2011) 105 [arXiv:1011.1167] [INSPIRE].

[31] L. Altenkort, A.M. Eller, O. Kaczmarek, L. Mazur, G.D. Moore and H.-T. Shu, *Sphaleron rate from Euclidean lattice correlators: An exploration*, *Phys. Rev. D* **103** (2021) 114513 [arXiv:2012.08279] [INSPIRE].

[32] L. Altenkort, A.M. Eller, O. Kaczmarek, L. Mazur, G.D. Moore and H.-T. Shu, *Lattice QCD noise reduction for bosonic correlators through blocking*, *Phys. Rev. D* **105** (2022) 094505 [arXiv:2112.02282] [INSPIRE].

[33] J.S. Langer, *Statistical theory of the decay of metastable states*, *Annals Phys.* **54** (1969) 258 [INSPIRE].

[34] I. Affleck, *Quantum Statistical Metastability*, *Phys. Rev. Lett.* **46** (1981) 388 [INSPIRE].

[35] A.D. Linde, *Fate of the False Vacuum at Finite Temperature: Theory and Applications*, *Phys. Lett. B* **100** (1981) 37 [INSPIRE].

[36] A.D. Linde, *Decay of the False Vacuum at Finite Temperature*, *Nucl. Phys. B* **216** (1983) 421 [*Erratum ibid.* **223** (1983) 544] [INSPIRE].

[37] S.R. Coleman, *The Fate of the False Vacuum. 1. Semiclassical Theory*, *Phys. Rev. D* **15** (1977) 2929 [*Erratum ibid.* **16** (1977) 1248] [INSPIRE].

[38] C.G. Callan, Jr. and S.R. Coleman, *The Fate of the False Vacuum. 2. First Quantum Corrections*, *Phys. Rev. D* **16** (1977) 1762 [INSPIRE].

[39] P.B. Arnold and L.D. McLerran, *The Sphaleron Strikes Back*, *Phys. Rev. D* **37** (1988) 1020 [INSPIRE].

JHEP01(2023)155

[40] P.B. Arnold and L.D. McLerran, *Sphalerons, Small Fluctuations and Baryon Number Violation in Electroweak Theory*, *Phys. Rev. D* **36** (1987) 581 [INSPIRE].

[41] R. Narayanan and H. Neuberger, *Infinite N phase transitions in continuum Wilson loop operators*, *JHEP* **03** (2006) 064 [hep-th/0601210] [INSPIRE].

[42] M. Lüscher, *Properties and uses of the Wilson flow in lattice QCD*, *JHEP* **08** (2010) 071 [*Erratum ibid.* **03** (2014) 092] [arXiv:1006.4518] [INSPIRE].

[43] G.D. Moore, *Measuring the broken phase sphaleron rate nonperturbatively*, *Phys. Rev. D* **59** (1999) 014503 [hep-ph/9805264] [INSPIRE].

[44] http://luscher.web.cern.ch/luscher/openQCD/index.html.

[45] B. De Palma, M. Erba, L. Mantovani and N. Mosco, *A python program for the implementation of the* Γ*-method for Monte Carlo simulations*, *Comput. Phys. Commun.* **234** (2018) 294 [arXiv:1703.02766] [INSPIRE].

[46] A. Francis, O. Kaczmarek, M. Laine, T. Neuhaus and H. Ohno, *Critical point and scale setting in* SU(3) *plasma: An update*, *Phys. Rev. D* **91** (2015) 096002 [arXiv:1503.05652] [INSPIRE].

[47] Y. Burnier et al., *Thermal quarkonium physics in the pseudoscalar channel*, *JHEP* **11** (2017) 206 [arXiv:1709.07612] [INSPIRE].

[48] J. Ambjørn and A. Krasnitz, *The Classical sphaleron transition rate exists and is equal to* $1.1(\alpha_w T)^4$, *Phys. Lett. B* **362** (1995) 97 [hep-ph/9508202] [INSPIRE].

[49] G.D. Moore and K. Rummukainen, *Classical sphaleron rate on fine lattices*, *Phys. Rev. D* **61** (2000) 105008 [hep-ph/9906259] [INSPIRE].

[50] M. Laine and Y. Schröder, *Two-loop QCD gauge coupling at high temperatures*, *JHEP* **03** (2005) 067 [hep-ph/0503061] [INSPIRE].

[51] R.V. Harlander and T. Neumann, *The perturbative QCD gradient flow to three loops*, *JHEP* **06** (2016) 161 [arXiv:1606.03756] [INSPIRE].

[52] A. Ramos and S. Sint, *Symanzik improvement of the gradient flow in lattice gauge theories*, *Eur. Phys. J. C* **76** (2016) 15 [arXiv:1508.05552] [INSPIRE].

JHEP01(2023)155